THE EIGENMODE PROJECTION TECHNIQUE: A NOVEL NUMERICAL ELECTROMAGNETIC METHOD

Mamdouh H. Nasr

Electronics and Electrical Communications Engineering Department
Faculty of Engineering at Cairo University

To my family and friends

Acknowledgment

In the name of Allah the most merciful the most gracious; all thanks to Allah the Lord of the Heavens and Earth and peace be upon Mohamed and his companions. I wish to express my gratitude to Dr. Tamer Abuelfadl and Dr. Islam Eshrah who were very helpful and offered invaluable assistance, support, guidance and constant care. I also thank Dr. Essam El-Diwany for his valuable effort in the revision of this manuscript.

Many thanks to my friends for their support and help through the duration of this work and through my whole life.

My deepest gratitude to my family. For my whole life, they encouraged me, inspired me, and sacrificed their lifes to make me a better person. Without their encouragement, I would not have gone this far.

Mamdouh

Abstract

AN eigenmode projection technique is employed to solve different electromagnetic problems making use of the solenoidal and irrotational eigenmodes of a canonical cavity. The technique is adopted to solve two classes of electromagnetic problems.

First, electromagnetic scattering by dielectric objects with complex dielectric constant is addressed, where a fictitious canonical cavity is chosen to enclose the scatterer, and the fields are expanded in terms of the complete set of the cavity solenoidal and irrotational eigenmodes. The fields in Maxwell's equations inside the enclosed region are then expanded using cavity eigenmodes. Mode projections are then performed making use of modes orthogonality, where the scatterer couples the canonical cavity modes. The fictitious cavity surface is regarded as a port excited by the incident wave, and the cavity fields and the port fields are then matched on the surface. Finally, a set of equations for the eigenmodes and scattered field amplitudes are solved together. The frequency independent feature of the eigenmodes, which represents Fourier type expansion functions, generates frequency independant matrices. This is exploited to provide a solution over a wide range of frequencies efficiently without the need of filling and inverting all the system of matrices, and the encountered numerical integrations are only evaluated once, with their values used at all frequencies. The technique also lends itself to problems where variations of the same structure are to be analyzed, with modifications that are not necessarily small as long as they are bound by the baseline canonical cavity with the encountered numerical integrations evaluated only for the added/subtracted volume.

Second, electromagnetic resonance in an arbitrary conducting cavity is solved, by projecting the cavity fields on the solenoidal and irrotational canonical modes, ending up with an eigenvalue problem with direct separation of the physical modes and spurious modes. The proposed formulation is verified for the special case of body-of-revolution cavities used in particle accelerators.

Contents

List of Tables

List of Figures

List of Symbols and Abbreviations

Mathematical Symbols

$\mathscr{D}$, **D** Electric flux desinty vector in time domain, frequency domain representation.

$\mathscr{H}$, **H** Magnetic field vector in time domain, frequency domain representation.

$\mathscr{J}$, **J** Electric current vector in time domain, frequency domain representation.

$\mathscr{M}$, **M** Magnetic current vector in time domain, frequency domain representation.

ρ_e Electric charge density.

ρ_m Magnetic charge density.

$\mathbf{E}_n$ Solenoidal electric field eigenmodes.

$\mathbf{H}_n$ Solenoidal magnetic field eigenmodes.

$a_n(t)$, a_n Solenoidal electric field coefficient in time domain, frequency domain representation.

$b_n(t)$, b_n Solenoidal magnetic field coefficient in time domain, frequency domain representation.

$\mathbf{F}_\alpha$ Irrotational electric field eigenmodes.

$\mathbf{G}_\lambda$ Irrotational magnetic field eigenfunctions.

$f_\alpha(t)$, f_α Irrotational electric field coefficient in time domain, frequency domain representation.

$g_\lambda(t)$, g_λ Irrotational magnetic field coefficient in time domain, frequency domain representation.

ϕ_α Electric potential eigenfunction.

ψ_λ Magnetic potential eigenfunction.

k, k_n Wavenumber, eigenvalues for the solenoidal fields.

l_α, l_λ Irrotatioanl electric, magnetic field eigenvalue.

μ_0, μ_r Permeability of vaccum, relative permiability.

ε_0, ε_r Permitivity of vaccum, relative permitivity.

η, η_n Intrinsic impedance of the medium, factional energy of the nth eigenmode.

σ Conductivity.

$\mathbf{r}$ Arbitrary position inside the domsin of volume V_t.

t Time.

Abbreviations

CEM Computational electromagnetics.

EPT Eigenmode Projection Technique.

FDTD Finite difference time domain.

RF Radio frequency.

LINAC Linear accelerator.

MoM Method of moments.

PEC Perfect electric conductor.

PMC Perfect magnetic conductor.

TE Transverse electric.

TM Transverse magnetic.

Chapter 1

Introduction

ELECTROMAGNETIC field expansion using cavity modes was first introduced by Slater in [1], where solenoidal and irrotational cavity eigemodes, forming a complete orthogonal set, were used to represent fields inside cavities. Kurokawa [2] then modified Slater's work by introducing the irrotational magnetic field. Further investigations of cavity eigenmode expansion were made to fully understand its properties in [3–5] and address numerous applications including microwave filters and high power applications [6].

The concept of modal expansion was previously applied to guided and unguided problems [7–10]. Also, it was combined with conventional techniques such as the finite-difference time-domain method (FDTD) [11], the finite element method (FEM) [12], and the integral equations using moment method (MoM) [13] to produce new hybrid methods for the solution of electromagnetic problems. Recently, an eigenmode projection technique (EPT) was introduced to analyze microwave cavities [14] as well as waveguide discontinuities [15], and proved to be quite efficient in the analysis of such problems with the occurrence, however, of some spurious (non-physical) modes that appear in the solution of resonance problems of arbitrary conducting cavities.

In this work, the EPT is applied to problems of electromagnetic scattering from dielectric objects with complex dielectric constant as well as resonance problems in arbitrary conducting cavities with direct spurious mode elimination. With available formulations both in time and frequency domain, the EPT will be shown to have automatic and natural choice of the basis functions, being the eigenmodes of an enclosing fictitious canonical cavity. In addition, the EPT has no singularity extraction problems and does not require special treatment for the domain truncation in case of free-space scattering problems. Also, the solution procedure involves the generation of a number of matrices, which are generally frequency independent. This directly translates to efficient analysis over a wide range of frequencies. Moreover, modifications to a baseline object material and shape enclosed in the same canonical cavity are readily analyzed by considering only integrals over the added/subtracted geometries.

This thesis is arranged as follows:

Chapter II: a quick overview on computational electromagnetics, is presented, highlighting the disadvantages of conventional techniques. Then, the eigenmode expansion is introduced illustrating its basic concepts and mathematical framework. Then, a formulation of Maxwell's equations in terms of eigemodes projections and surface currents is introduced to obtain electromagnetic problems solution using the eigenmode projection technique.

Chapter III: electromagnetic scattering by dielectric objects with complex dielectric constant is addressed, where a fictitious canonical cavity is chosen to enclose the scatterer, and the fields are expanded in terms of the complete set of the cavity solenoidal and irrotational eigenmodes. The fields in Maxwell's equations inside the enclosed region are then expanded using cavity eigenmodes. Mode projections are then performed making use of modes orthogonality, where the scatterer couples the canonical cavity modes. The fictitious cavity surface is regarded as a port excited by the incident wave, and the cavity fields and the port fields are then matched on the surface. Finally, a set of equations for the eigenmodes and scattered field amplitudes are resulted and solved together. Unique features of the EPT will be demonstrated. The technique will also be validated against analytical results as well as results obtained using other numerical methods.

Chapter IV: resonance of arbitrary-shaped cavities is analyzed in this chapter using the EPT, where a new approach is introduced with direct and efficient spurious modes separation by modeling the cavity walls by a highly conductive material. First, the general derivation is introduced, then results for canonical and arbitrary-shaped cavities are verified using analytical formulas and CST commercial simulation package solution.

Chapter 2

On the Eigenmode Expansion of Cavity Fields

In this chapter, a quick overview on computational electromagnetics, highlighting the disadvantages in conventional techniques, is presented. Then, the eigenmode expansion is introduced illustrating its basic concepts and mathematical framework. Then, a formulation of Maxwell's equations in terms of eigemodes projections and surface currents is introduced to obtain electromagnetic problems solution using the eigenmode projection technique.

2.1 Computational Electromagnetics: An Overview

With the advent of high-speed computers with large computational and storage resources, computational electromagnetic techniques have dramatically evolved and become the norm in solving electromagnetic problems. The real power of computational electromagnetics (CEM) is in providing the solution of many problems with no analytical closed solution, which is the case for most real-life complex problems. CEM are utilized in many applications such as scattering, resonance problems, microwave filters, high power devices, and optical devices.

Many numerical techniques were proposed utilizing different approaches in solving electromagnetic problems. Such techniques can be categorized into: partial domain methods, which require the discretization of only part of the solution domain, such as the integral equations using moment method [16] and entire domain methods, which require the discretization of the whole domain including certain absorbing boundaries, such as the FDTD) [17] as illustrated below.

Integral Equations using Moment Method (MoM)

In the MoM, the surface equivalence principle is used by providing equivalent electric and magnetic surface currents over arbitrary geometries. These currents are then segmented and basis functions are defined over these segments. Testing functions are then projected over these basis functions. Finally, a matrix equation comprises the unknown current coefficients is built and solved using the appropriate basis functions and weighting functions. The use of Greens functions (in different forms) is essential in this technique. The MoM provides the solution in frequency domain and is suitable for scattering and antenna problems where no domain truncation is needed in this method.

For the MoM, the choice of the basis functions is not automatic and there is no way to know the best basis functions to use specially for general purpose solvers. Also, the matrix filling process, which incorporates evaluation of singular integrals and singularity extraction, stands out. Moreover, the frequency dependence of the MoM matrix requires evaluating and inverting it at each frequency point of the frequency sweep plan, which is a very time consuming process if wideband analysis is required.

Finite Difference Time Domain (FDTD)

FDTD is widely used in general purpose solvers. It is a simple and straightforward method that is based on domain truncation and the representation of Maxwell's equations in difference form in the time domain. For the FDTD method, the entire domain of the problem has to be discretized and properly truncated using absorbing boundaries or matched layers to emulate unbounded regions in case of solving scattering problems. Also, it requires meshing and discretization of the whole domain, which results in prohibitively large computations.

Thus, conventional numerical techniques are mainly based on geometrical discretization and the choice of some basis functions to solve the problem under consideration. Typically, the choice of the basis functions is arbitrary, especially for general-purpose solvers, not to mention other problems that depends on the technique such as singularity extraction, domain truncation...etc.

In the next section, the framework of the eigenmode projection technique (EPT) will be introduced, which will be shown to address many of problems encountered in conventional techniques, and offers other advantages that come about as a natural consequence of its derivation.

2.2 The Eigenmode Expansion

The use of cavity eigenmodes to represent electric and magnetic fields is detailed in this section, with rigorous mathematical framework, that will lay the foundation for the proposed EPT.

2.2.1 Helmholtz Theorem

Helmholtz's theorem [18], also known as the fundamental theorem of vector calculus, states that any vector field $\mathbf{F}$ in three dimensions can be resolved into the sum of an irrotational (curl-free) vector field and a solenoidal (divergence-free) vector field; this is also known as the Helmholtz decomposition. The irrotational component is represented by the scalar potential ϕ, while the divergenceless component is represented by the curl of an auxiliary vector potential $\mathbf{A}$, viz.

$$\mathbf{F} = \nabla \times \mathbf{A} + \nabla\phi \tag{2.1}$$

which is clearly based on the mathematical identities: $\nabla \times \nabla\phi = 0$, $\nabla \cdot \nabla \times \mathbf{A} = 0$. Generally, a vector-field is fully described by the two components, to within an arbitrary constant.

2.2.2 Eigenmode Expansion

The eigenmode expansion provides a representation of the electric and magnetic fields in a certain region in space enclosed by a canonical cavity in terms of the cavity eigenmodes. For an arbitrary-lossless cavity of volume V_t and bounded by a surface S_t as shown in Fig. 2.1, the eigenmodes are divided into two categories: solenoidal and irrotational. The surface S_t is assumed to be partly perfect electric conducting S_{PE} and partly perfect magnetic conducting S_{PM}. From the boundary conditions and the geometry of the cavity, these eigenmodes can be determined as a set of solenoidal (divergence-free) and irrotational (curl-free) modes forming a complete orthogonal set [1, 2] that could represent the cavity electric and magnetic fields as

$$\mathscr{E}(\mathbf{r};t) = \sum_n a_n(t)\mathbf{E}_n(\mathbf{r}) + \sum_\alpha f_\alpha(t)\mathbf{F}_\alpha(\mathbf{r}), \tag{2.2}$$

$$\mathscr{H}(\mathbf{r};t) = \sum_n b_n(t)\mathbf{H}_n(\mathbf{r}) + \sum_\lambda g_\lambda(t)\mathbf{G}_\lambda(\mathbf{r}). \tag{2.3}$$

where $\mathbf{E}_n$, $\mathbf{H}_n$ are the solenoidal electric and magnetic eigenmodes, while $\mathbf{F}_\alpha$, $\mathbf{G}_\lambda$ are the irrotational electric and magnetic eigenmodes.

In general, both the curl and divergence of the electric field are non-zero , and thus it is expanded in terms of both modes: the solenoidal eigenmodes governed by

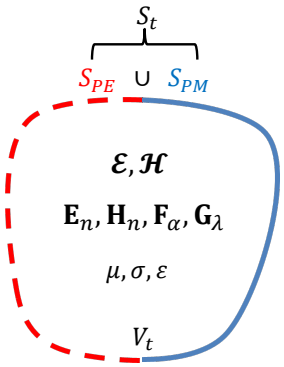

Figure 2.1: A general cavity defined by the volume V_t , bounding surface S_t, and its orthogonal eigenfunctions.

$$\left.\begin{aligned}\left(\nabla^2 + k_n^2\right)\mathbf{E}_n &= 0\\ \nabla\cdot\mathbf{E}_n &= 0\end{aligned}\right\}, \quad \text{in } V_t$$
$$\hat{\mathbf{n}}\times\mathbf{E}_n = 0, \quad \text{on } S_{PE}$$
$$\hat{\mathbf{n}}\cdot\mathbf{E}_n = 0, \quad \text{on } S_{PM} \tag{2.4}$$

and the irrotational modes having

$$\left.\begin{aligned} l_\alpha\mathbf{F}_\alpha &= \nabla\phi_\alpha\\ \left(\nabla^2 + l_\alpha^2\right)\phi_\alpha &= 0\\ \nabla\times\mathbf{F}_\alpha &= 0\end{aligned}\right\}, \quad \text{in } V_t$$
$$\hat{\mathbf{n}}\times\mathbf{F}_\alpha = 0,\ \phi_\alpha = 0, \quad \text{on } S_{PE}$$
$$\hat{\mathbf{n}}\cdot\mathbf{F}_\alpha = 0,\ \frac{\partial\phi_\alpha}{\partial n} = 0, \quad \text{on } S_{PM} \tag{2.5}$$

where $\hat{\mathbf{n}}$ is the outward normal vector to the canonical cavity surface and k_n, l_α are the eigenvalues for the solenoidal and irrotational electric field, respectively.

Similarly, using the solenoidal eigenmodes with

$$\left.\begin{aligned}\left(\nabla^2 + k_n^2\right)\mathbf{H}_n &= 0\\ \nabla\cdot\mathbf{H}_n &= 0\end{aligned}\right\}, \quad \text{in } V_t$$
$$\hat{\mathbf{n}}\cdot\mathbf{H}_n = 0, \quad \text{on } S_{PE}$$
$$\hat{\mathbf{n}}\times\mathbf{H}_n = 0, \quad \text{on } S_{PM} \tag{2.6}$$

and the irrotational ones having

$$\left.\begin{aligned} w_\lambda \mathbf{G}_\alpha &= \nabla \psi_\lambda \\ \left(\nabla^2 + w_\lambda^2\right) \psi_\lambda &= 0 \\ \nabla \times \mathbf{G}_\lambda &= 0 \end{aligned}\right\}, \quad \text{in } V_t$$

$$\hat{\mathbf{n}} \cdot \mathbf{G}_\lambda = 0, \frac{\partial \psi_\lambda}{\partial n} = 0, \quad \text{on } S_{PE}$$

$$\hat{\mathbf{n}} \times \mathbf{G}_\lambda = 0, \psi_\lambda = 0, \quad \text{on } S_{PM}$$

where k_n, w_λ are the eigenvalues for the irrotational electric and magnetic fields, respectively.

These eigen modes are frequency independent and represent a sort of spatial fourier expansion basis functions for the fields inside the cavity with the specified boundary conditions.

The irrotational magnetic eigenmodes were introduced by Kurokawa in [2] as a necessary component to form a complete expansion for the magnetic field. This can be explained as follows: due to the truncation of the medium by the canonical fictitious cavity, some magnetic field closed lines could be truncated by the cavity. These field lines enters the canonical cavity through a part of S_t and returns it through the another part of S_t. Thus to accommodate for the field lines truncation, a magnetic charge $+|\hat{\mathrm{n}} \cdot \mathscr{B}|$ should be placed at the entrance of the field lines through S_t, and another charge $-|\hat{\mathrm{n}} \cdot \mathscr{B}|$ at their exit from S_t With the presence of these magnetic charges, the irrotational eigenmodes of the magnetic field are needed to have full representation of the magnetic field inside the cavity region.

2.2.2.1 Relation Between the Solenoidal Electric and Magnetic Eigenmodes

The eigenvalues for the solenoidal electric and magnetic eigenmodes, $\mathbf{E}_n$ and $\mathbf{H}_n$ are named k_n since they are, in fact, equal [18]. Furthermore, it can be shown that

$$\nabla \times \mathbf{E}_n = k_n \mathbf{H}_n, \quad \nabla \times \mathbf{H}_n = k_n \mathbf{E}_n, \quad \text{in } V_t \tag{2.7}$$

The curl of the first relation gives

$$\nabla \times \nabla \times \mathbf{E}_n = \nabla \left(\nabla \cdot \mathbf{E}_n\right) - \nabla^2 \mathbf{E}_n = -\nabla^2 \mathbf{E}_n = k_n \nabla \times \mathbf{H}_n = k_n^2 \mathbf{E}_n \tag{2.8}$$

Thus, the solenoidal modes satisfy homogeneous Helmholtz equation, i.e. it is satisfying Helmholtz equation of electric field $\left(\nabla^2 + k_n^2\right) \mathbf{E}_n = 0$. This can be also shown for the magnetic field eigenmodes, since

$$\nabla \times \nabla \times \mathbf{H}_n = \nabla \left(\nabla \cdot \mathbf{H}_n\right) - \nabla^2 \mathbf{H}_n = -\nabla^2 \mathbf{H}_n = k_n \nabla \times \mathbf{E}_n = k_n^2 \mathbf{H}_n \tag{2.9}$$

2.2.2.2 Orthogonality of Eigenmodes

As proven in [18], the cavity eigenmodes discussed above form a complete orthonormal set having

$$\left.\begin{array}{r} \int_{V_t} \mathbf{Q}_m(\mathbf{r}) \cdot \mathbf{Q}_n(\mathbf{r}) dv \\ \int_{V_t} U_m U_n dv \end{array}\right\} = \delta_{mn} \tag{2.10}$$

where δ_{mn} is the Kronecker delta, $\mathbf{Q}$ stands for $\mathbf{E}$, $\mathbf{H}$, $\mathbf{F}$, $\mathbf{G}$ and U for ψ, ϕ. Also, projections between solenoidal and irrotational modes vanish.

2.2.2.3 Expansion of the Fields Derivatives using the Eigenmodes and Surface Currents

Assuming non-homogeneous dielectric medium, It was shown in [19], following the same procedure as in [1] and taking into consideration the irrotational magnetic fields introduced in [2], that $\nabla \times \mathscr{E}(\mathbf{r};t)$ may be carefully obtained using the following relation

$$\nabla \times \mathscr{E}(\mathbf{r};t) = \sum_n \left[k_n a_n(t) + \oint_{S_t} (\mathscr{E}(\mathbf{r};t) \times \mathbf{H}_n(\mathbf{r})) \cdot ds \right] \mathbf{H}_n(\mathbf{r}) + \sum_\lambda \left[\oint_{S_t} (\mathscr{E}(\mathbf{r};t) \times \mathbf{G}_\lambda(\mathbf{r})) \cdot ds \right] \mathbf{G}_\lambda(\mathbf{r}) \tag{2.11}$$

and should not be mistakenly obtained in the presence of port fields by taking the curl of the expansion in (2.2) and making use of (2.7), resulting in $\sum_n k_n a_n^t(t) \mathbf{H}_n(\mathbf{r})$.

Similarly for $\nabla \times \mathscr{H}(\mathbf{r};t)$,

$$\nabla \times \mathscr{H}(\mathbf{r};t) = \sum_n \left[k_n b_n(t) + \oint_{S_t} (\mathscr{H}(\mathbf{r};t) \times \mathbf{E}_n(\mathbf{r})) \cdot ds \right] \mathbf{E}_n(\mathbf{r}) + \sum_\alpha \left[\oint_{S_t} (\mathscr{H}(\mathbf{r};t) \times \mathbf{F}_\alpha(\mathbf{r})) \cdot ds \right] \mathbf{F}_\alpha(\mathbf{r}) \tag{2.12}$$

In other words, a sum of terms involving surface integrals will appear in the expansion of $\nabla \times \mathscr{E}(\mathbf{r};t)$ and $\nabla \times \mathscr{H}(\mathbf{r};t)$. In electromagnetic scattering problems (the subject of the next chapter), these terms will represent the coupling between the (fictitious) cavity eigenmodes and the outer (port) modes and result from the field discontinuity at the canonical fictitious cavity surface.

It is to be noted that if the fictitious cavity is considered with PM walls the surface integral term, containing $\mathbf{H}_n$ in (2.11) vanishes. On the other hand, if the fictitious cavity is considered with PE walls the surface integral term, containing $\mathbf{E}_n$ in (2.12) vanishes. For the case of PM

wall, although the tangential components of $\mathbf{H}_n$ vanish at the surface of the cavity, the port magnetic field couples to the $\mathbf{E}_n$ fields in (2.12) . Corresponding argument holds for (2.11) for the case with PE wall.

Also, the divergence of electric and magnetic fields are expanded, in a similar manner, in terms of scalar potentials as follows:

$$\nabla \cdot \mathscr{D}(\mathbf{r};t) = \varepsilon_0 \sum_{\alpha} \left[\oint_{S_t} (\varepsilon_r(\mathbf{r}) \mathscr{E}(\mathbf{r};t) \phi_\alpha(\mathbf{r})) \cdot ds - l_\alpha \int_{V_t} \varepsilon_r(\mathbf{r}) \mathscr{E}(\mathbf{r};t) \cdot \mathbf{F}_\alpha(\mathbf{r}) dv \right] \phi_\alpha(\mathbf{r}) \quad (2.13)$$

$$\nabla \cdot \mathscr{B}(\mathbf{r};t) = \mu_0 \nabla \cdot \mu_r(\mathbf{r}) \mathscr{H}(\mathbf{r};t) = \mu_0 \sum_{\lambda} \left[\oint_{S_t} (\mu_r(\mathbf{r}) \mathscr{H}(\mathbf{r};t) \psi_\lambda(\mathbf{r})) \cdot d\mathbf{s} \right.$$
$$\left. - w_\lambda \int_{V_t} \mu_r(\mathbf{r}) \mathscr{H}(\mathbf{r};t) \cdot \mathbf{G}_\lambda(\mathbf{r}) dv \right] \psi_\lambda(\mathbf{r}) \quad (2.14)$$

With the above expressions for the divergence and curl of the electric and magnetic fields, Maxwell's equations can be recast in the form that will suit the purpose of this study.

2.2.3 Maxwell's Equations using the Eigenmode Expansion with Mode Projections

Maxwell's equation in the time domain are

$$\nabla \times \mathscr{E}(\mathbf{r};t) = -\frac{\partial \mathscr{B}(\mathbf{r};t)}{\partial t} - \mathscr{M}(\mathbf{r};t) \quad (2.15)$$

$$\nabla \times \mathscr{H}(\mathbf{r};t) = \frac{\partial \mathscr{D}(\mathbf{r};t)}{\partial t} + \mathscr{J}_i(\mathbf{r};t) + \mathscr{J}_c(\mathbf{r};t) \quad (2.16)$$

$$\nabla \cdot \mathscr{D}(\mathbf{r};t) = \rho_e(\mathbf{r};t) \quad (2.17)$$

$$\nabla \cdot \mathscr{B}(\mathbf{r};t) = \rho_m(\mathbf{r};t) \quad (2.18)$$

where $\mathscr{J}_i(\mathbf{r};t)$ and $\mathscr{J}_c(\mathbf{r};t)$ are the impressed and conduction currents, respectively. With the above expressions for the divergence and curl of the electric and magnetic fields, Maxwell's equations can be recast in the form that will suit the purpose of this study.

$$\sum_n \left[k_n a_n(t) + \oint_{S_t} (\mathscr{E}(\mathbf{r};t) \times \mathbf{H}_n(\mathbf{r})) \cdot ds \right] \mathbf{H}_n(\mathbf{r}) - \sum_\lambda \left[\oint_{S_t} (\mathscr{E}(\mathbf{r};t) \times \mathbf{G}_\lambda(\mathbf{r})) \cdot ds \right] \mathbf{G}_\lambda(\mathbf{r})$$
$$= -\frac{\partial}{\partial t} \mu_0 \mu_r(\mathbf{r}) \left[\sum_m b_m(t) \mathbf{H}_m(\mathbf{r}) + \sum_{\lambda'} g_{\lambda'}(t) \mathbf{G}_{\lambda'}(\mathbf{r}) \right] - \mathscr{M}(\mathbf{r};t) \quad (2.19)$$

$$\sum_n \left[k_n b_n(t) + \oint_{S_t} (\mathscr{H}(\mathbf{r};t) \times \mathbf{E}_n(\mathbf{r})) \cdot ds \right] \mathbf{E}_n(\mathbf{r}) + \sum_\alpha \left[\oint_{S_t} (\mathscr{H}(\mathbf{r};t) \times \mathbf{F}_\alpha(\mathbf{r})) \cdot ds \right] \mathbf{F}_\alpha(\mathbf{r})$$
$$= \left[\varepsilon_0 \varepsilon_r(\mathbf{r}) \frac{\partial}{\partial t} + \sigma(\mathbf{r}) \right] \left[\sum_m a_m(t) \mathbf{E}_m(\mathbf{r}) + \sum_{\alpha'} f_{\alpha'}(t) \mathbf{F}_{\alpha'}(\mathbf{r}) \right] + \mathscr{J}_i(\mathbf{r};t) \quad (2.20)$$

$$\sum_\alpha \left[\oint_{S_t} (\varepsilon_r(\mathbf{r}) \mathscr{E}(\mathbf{r};t) \phi_\alpha) \cdot ds - l_\alpha \left[\sum_m a_m(t) \int_{V_t} \varepsilon_r(\mathbf{r}) \mathbf{E}_m(\mathbf{r}) \cdot \mathbf{F}_\alpha(\mathbf{r}) dv \right. \right.$$
$$\left. \left. + \sum_{\alpha'} f_{\alpha'}(t) \int_{V_t} \varepsilon_r(\mathbf{r}) \mathbf{F}_\alpha(\mathbf{r}) \cdot \mathbf{F}_{\alpha'}(\mathbf{r}) dv \right] \right] \phi_\alpha(\mathbf{r}) = \frac{1}{\varepsilon_0} \rho_e(\mathbf{r};t) \quad (2.21)$$

$$\sum_\lambda \left[\oint_{S_t} (\mu_r(\mathbf{r}) \mathscr{H}(\mathbf{r};t) \psi_\lambda(\mathbf{r})) \cdot ds - w_\lambda \left[\sum_m b_m(t) \int_{V_t} \mu_r(\mathbf{r}) \mathbf{G}_\lambda(\mathbf{r}) \cdot \mathbf{H}_m(\mathbf{r}) dv \right. \right.$$
$$\left. \left. + \sum_{\lambda'} g_{\lambda'}(t) \int_{V_t} \mu_r(\mathbf{r}) \mathbf{G}_\lambda(\mathbf{r}) \cdot \mathbf{G}_{\lambda'}(\mathbf{r}) dv \right] \right] \psi_\lambda(\mathbf{r}) = \frac{1}{\mu_0} \rho_m(\mathbf{r};t) \quad (2.22)$$

Projecting (2.19) on $\mathbf{H}_n$ and making use of the orthogonality outlines in (2.10) yields a set of equations

$$k_n a_n(t) + \oint_{S_t} (\mathscr{E}(\mathbf{r};t) \times \mathbf{H}_n(\mathbf{r})) \cdot ds = -\mu_0 \left[\sum_n \frac{\partial b_n(t)}{\partial t} \int_{V_t} \mu_r(\mathbf{r}) \mathbf{H}_n(\mathbf{r}) \cdot \mathbf{H}_m(\mathbf{r}) dv \right.$$
$$\left. + \sum_{\lambda'} \frac{\partial g_{\lambda'}(t)}{\partial t} \int_{V_t} \mu_r(\mathbf{r}) \mathbf{H}_n(\mathbf{r}) \cdot \mathbf{G}_{\lambda'}(\mathbf{r}) dv \right] - \int_{V_t} \mathscr{M}(\mathbf{r};t) \cdot \mathbf{H}_n(\mathbf{r}) dv \quad (2.23)$$

Similarly (2.20) is projected on $\mathbf{E}_n$, (2.21) on $\phi_\alpha(\mathbf{r})$ and (2.22) on $\psi_\lambda(\mathbf{r})$, resulting in the following equations

$$k_n b_n(t) + \oint_{S_t} (\mathscr{H}(\mathbf{r};t) \times \mathbf{E}_n(\mathbf{r})) \cdot ds = \varepsilon_0 \left[\sum_m \frac{\partial a_m(t)}{\partial t} \int_{V_t} \varepsilon_r(r) \mathbf{E}_n(\mathbf{r}) \cdot \mathbf{E}_m(\mathbf{r}) dv \right.$$
$$\left. + \sum_{\alpha'} \frac{\partial f_{\alpha'}(t)}{\partial t} \int_{V_t} \varepsilon_r(\mathbf{r}) \mathbf{E}_n(\mathbf{r}) \cdot \mathbf{F}_{\alpha'}(\mathbf{r}) dv \right] + \left[\sum_m a_m(t) \int_{V_t} \sigma(\mathbf{r}) \mathbf{E}_n(\mathbf{r}) \cdot \mathbf{E}_m(\mathbf{r}) dv \right.$$
$$\left. + \sum_{\alpha'} f_{\alpha'}(t) \int_{V_t} \sigma(\mathbf{r}) \mathbf{E}_n(\mathbf{r}) \cdot \mathbf{F}_{\alpha'}(\mathbf{r}) dv \right] + \int_{V_t} \mathscr{J}(\mathbf{r};t) \cdot \mathbf{E}_n(\mathbf{r}) dv \quad (2.24)$$

$$\oint_{S_t} (\varepsilon_r(\mathbf{r}) \mathscr{E}(\mathbf{r};t) \phi_\alpha) \cdot ds - l_\alpha \left[\sum_m a_m(t) \int_{V_t} \varepsilon_r(\mathbf{r}) \mathbf{E}_m(\mathbf{r}) \cdot \mathbf{F}_\alpha(\mathbf{r}) dv \right.$$
$$\left. + \sum_{\alpha'} f_{\alpha'}(t) \int_{V_t} \varepsilon_r(\mathbf{r}) \mathbf{F}_\alpha(\mathbf{r}) \cdot \mathbf{F}_{\alpha'}(\mathbf{r}) dv \right] = \frac{1}{\varepsilon_0} \int_{V_t} \rho_e(\mathbf{r};t) \phi_\alpha(\mathbf{r}) dv \quad (2.25)$$

$$\oint_{S_t} (\mu_r(\mathbf{r}) \mathscr{H}(\mathbf{r};t) \psi_\lambda(\mathbf{r})) \cdot ds - w_\lambda \left[\sum_m b_m(t) \int_{V_t} \mu_r(\mathbf{r}) \mathbf{G}_\lambda(\mathbf{r}) \cdot \mathbf{H}_m(\mathbf{r}) dv \right.$$
$$\left. + \sum_{\lambda'} g_{\lambda'}(t) \int_{V_t} \mu_r(\mathbf{r}) \mathbf{G}_\lambda(\mathbf{r}) \cdot \mathbf{G}_{\lambda'}(\mathbf{r}) dv \right] = \frac{1}{\mu_0} \int_{V_t} \rho_m(\mathbf{r};t) \psi_\lambda(\mathbf{r}) dv \quad (2.26)$$

Consequently, (2.23-2.26) represent a system of equations in the eigenmode coefficients $a_n(t)$, $b_n(t)$, $f_\alpha(t)$, and $g_\lambda(t)$.

It is important here to notice that, in case of homogeneously filled cavities, the constitutive parameters will be constant over the cavity volume, resulting in vanishing coupling between eigenmodes. For a non-homogenous dielectric profile, however, mode coupling will exist. In electromagnetic scattering problems, studied in the next chapter, coupling between cavity eigenmodes and the outer region will be achieved via the surface integrals. This is not the case in resonance problems, where there is no outer region.

Chapter 3

Electromagnetic Scattering Analysis Using the Eigenmode Projection Technique

ELECTROMAGNETIC scattering by dielectric objects with complex dielectric constant is addressed in this chapter, where a fictitious canonical cavity is chosen to enclose the scatterer, and the fields are expanded in terms of the complete set of the cavity solenoidal and irrotational eigenmodes. The fields in Maxwell's equations inside the enclosed region are then expanded using cavity eigenmodes. Mode projections are then performed making use of modes orthogonality, where the scatterer couples the canonical cavity modes. The fictitious cavity surface is regarded as a port excited by the incident wave, and the cavity fields and the port fields are then matched on the surface. Finally, a set of equations for the eigenmodes and scattered field amplitudes are solved together. Unique features of the EPT will be demonstrated. The technique will also be validated against analytical results as well as results obtained using other numerical methods.

3.1 Conceptual Framework

Analysis of electromagnetic scattering problems has received great attention due to their relevance in a wide range of applications. The scattering properties of different objects, ranging from electrically small to electrically huge ones, have been studied using different techniques with the goal of solving them both efficiently and accurately.

As previously illustrated, conventional numerical techniques are mainly based on geometrical discretization and the choice of some basis functions to solve the problem under consideration.

In this work, the solution domain is divided into two regions: an enclosure that encloses the scatterer and an outer space. This enclosure is chosen to be a fictitious canonical cavity, and the fields inside the cavity are expanded in terms of the cavity solenoidal and irrotational eigenmodes, which forms a complete orthogonal set, with certain mode amplitudes. On the other hand, the fields in the outer space, outside the fictitious canonical cavity, which constitute the incident and scattered fields are represented using angular harmonics expansion with another set of amplitudes referred to as the scattered coefficients. The fields in Maxwell's equations inside the enclosed region are then expanded using cavity eigenmodes. Mode projections are then performed making use of modes orthogonality, where the scatterer couples the canonical cavity modes. The fields at the two regions boundary are then matched. Finally, a set of equations for the eigenmodes and scattered field amplitudes are resulted and solved together.

In the next sections, the problem formulation will be described in detail starting with the field definitions for the inside and outside regions and ending with the required field coefficients. The frequency independent feature of the eigenmodes, which represent Fourier type expansion functions, generates frequency independant matrices. This is exploited to provide an efficient solution over a wide range of frequencies without the need of filling and inverting all the system of matrices and the numerical integrations are only evaluated once, with their values used at all frequencies. It will be shown also that the technique lends itself to problems, where variations of the same structure are to be analyzed, with the modifications not necessarily small as long as they are bound by the same canonical cavity.

3.2 Problem Formulation

Considering an arbitrarily shaped dielectric object excited by a uniform plane wave or some impressed sources as illustrated in Fig. 3.1, the solution procedure can be summarized as follows: First, a fictitious canonical cavity with perfect magnetic (PM) or perfect electric (PE) conducting boundary is chosen to enclose the scatterer. The cavity is chosen to be either cylindrical or spherical according to the problem under consideration, being either two dimensional (2D) or three dimensional (3D), respectively. Then, the fields are expanded in terms of the cavity solenoidal and irrotational eigenmodes, which are used in Maxwell's equations inside the enclosed region. The fictitious cavity surface is then regarded as a port excited by the incident and scattered waves, and the cavity fields and port fields are then matched by enforcing the boundary conditions on the cavity surface. The resulting matrix equations are then solved for the unknown field coefficients.

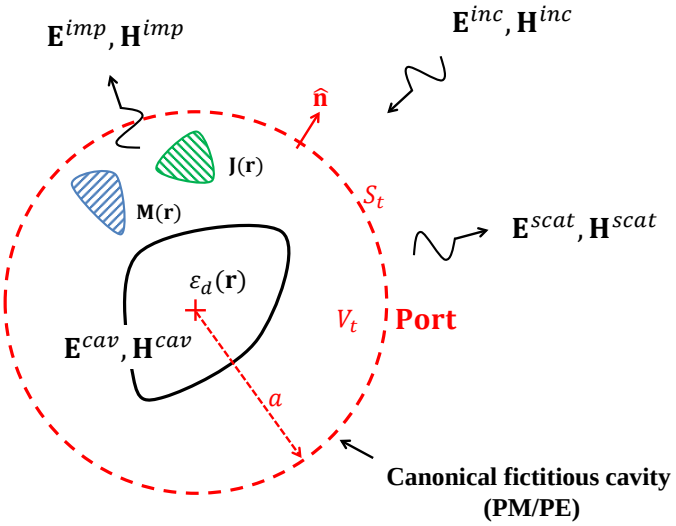

Figure 3.1: General scattering problem by an arbitrary dielectric object with permittivity function $\varepsilon_d(\mathbf{r})$. The object is enclosed by a canonical fictitious cavity with radius a , volume V_t and outer surface S_t.

3.2.1 Port Modes

The instantaneous total port field is the summation of the incident (of a plane wave), impressed (by sources), and the scattered fields at the canonical cavity boundary (port) as follows:

$$\mathscr{E}^{port}(\mathbf{a};t) = \mathscr{E}^{inc}(\mathbf{a};t) + \mathscr{E}^{imp}(\mathbf{a};t) + \mathscr{E}^{scat}(\mathbf{a};t) \tag{3.1}$$

$$\mathscr{H}^{port}(\mathbf{a};t) = -\frac{1}{\mu_0}\int_0^t \nabla \times \mathscr{E}^{port}(\mathbf{a};t')dt' \tag{3.2}$$

where $(\mathbf{a};t) = (a,\theta,\phi;t)$ and $\mathscr{E}^{imp}(\mathbf{a};t)$ is the field due to the impressed sources that could be inside or outside the canonical cavity, in the absence of the scatterer. Thus, this field is obtained using the free-space Green's function.

The port fields are expanded in terms of spatial angular harmonics with unknown amplitudes for the scattered harmonics.

3.2.2 Cavity Eigenmodes

The fields inside the cavity are represented by the previously mentioned cavity eigenmodes in (2.2-2.3) as follows:

$$\mathscr{E}^{cav}(\mathbf{r};t) = \sum_n a_n(t)\mathbf{E}_n(\mathbf{r}) + \sum_\alpha f_\alpha(t)\mathbf{F}_\alpha(\mathbf{r}), \tag{3.3}$$

$$\mathscr{H}^{cav}(\mathbf{r};t) = \sum_n b_n(t)\mathbf{H}_n(\mathbf{r}) + \sum_\lambda g_\lambda(t)\mathbf{G}_\lambda(\mathbf{r}). \tag{3.4}$$

It is important to emphasize that the solenoidal part of the electric and magnetic fields ($\mathbf{E}_n, \mathbf{H}_n$) is this part of the field that shows properties of wave propagation, and is usually regarded as the radiation field. On the other hand, the irrotational part of the fields ($\mathbf{F}_\alpha, \mathbf{G}_\lambda$) is similar to the electrostatic field resulting of a known distribution of charge. The only difference between this and electrostatic problem is that the charge distribution, and hence the field varies with time [1, pp. 472-473]. Needless to say, the infinite number of modes is truncated to N solenoidal modes and L, O irrotational electric and magnetic ones, respectively, upon adopting certain convergence criteria.

3.2.3 Application of Eigenmode Projections to Maxwell's Equations Inside the Fictitious Cavity

Applying eigenmode projections to Maxwell's equations inside the fictitious cavity results in (2.23-2.26). Casting these equations to the problem under consideration with lossless ($\sigma = 0$), non-magnetic ($\mu_r = 1$) material, yields the following system of equations

$$k_n a_n(t) + \oint_{S_t} \left(\mathscr{E}^{port}(\mathbf{a};t) \times \mathbf{H}_n(\mathbf{a})\right) \cdot ds = -\mu_0 \frac{\partial b_n(t)}{\partial t} - \int_{V_t} \mathscr{M}(\mathbf{r};t) \cdot \mathbf{H}_n(\mathbf{r}) dv, \tag{3.5}$$

$$k_n b_n(t) + \oint_{S_t} \left(\mathscr{H}^{port}(\mathbf{a};t) \times \mathbf{E}_n(\mathbf{a})\right) \cdot ds = \frac{\partial}{\partial t}\left[\sum_{n'} a_{n'}(t) \langle \mathbf{E}_n, \mathbf{E}_{n'} \rangle + \sum_{\alpha'} f_{\alpha'}(t) \langle \mathbf{E}_n, \mathbf{F}_{\alpha'} \rangle\right] + \int_{V_t} \mathscr{J}(\mathbf{r};t) \cdot \mathbf{E}_n(\mathbf{r}) dv, \tag{3.6}$$

$$\varepsilon_0 \oint_{S_t} \left(\mathscr{E}^{port}(\mathbf{a};t)\phi_\alpha(\mathbf{a})\right) \cdot ds - l_\alpha \left[\sum_{n'} a_{n'}(t) \langle \mathbf{E}_{n'}, \mathbf{F}_\alpha \rangle + \sum_{\alpha'} f_{\alpha'}(t) \langle \mathbf{F}_\alpha, \mathbf{F}_{\alpha'} \rangle\right] = \int_{V_t} \rho_e(\mathbf{r};t)\phi_\alpha(\mathbf{r}) dv, \tag{3.7}$$

$$\oint_{S_t} \left(\mathscr{H}^{port}(\mathbf{a};t)\psi_\lambda(\mathbf{a})\right)\cdot ds - w_\lambda g_\lambda(t) = \frac{1}{\mu_0}\int_{V_t}\rho_m(\mathbf{r};t)\psi_\lambda(\mathbf{r})dv, \tag{3.8}$$

where $\langle \mathbf{X}, \mathbf{Y}\rangle = \int_{V_t}\varepsilon(\mathbf{r})\mathbf{X}(\mathbf{r})\cdot\mathbf{Y}(\mathbf{r})dv$ with

$$\varepsilon(\mathbf{r}) = \begin{cases} \varepsilon_d(\mathbf{r}), & \text{inside dielectric} \\ \varepsilon_0, & \text{elsewhere} \end{cases}$$

and the impressed currents $\mathscr{J}$ and $\mathscr{M}$ and charges ρ_e and ρ_m appear only when there is a source inside the canonical cavity.

The previous time-domain derivations can be pursued to obtain instantaneous values for the scattered fields. Since the interest in this work, however, is the exploitation of the features of the frequency-domain formulation of the EPT, in the rest of this Chapter, a time-harmonic variation of the form $e^{j\omega t}$ will be assumed and the frequency domain will be adopted.

Consequently, the scattered electric field in frequency domain will be casted in the form $\mathbf{E}^{scat}(\mathbf{r}) = \sum_p a_p^{scat}\mathbf{e}_p(\mathbf{r})$, with $\mathbf{e}_p(\mathbf{r})$ being the angular harmonics of the scattered fields from cylindrical or spherical objects in case of 2D or 3D problems, respectively, with $p = 1, 2, \cdots M$ where M is the number of port modes under consideration, and a_p^{scat} the unknown amplitudes of the scattered harmonics. More details are provided in Appendix A and B for 2D and 3D problems, respectively.

It is should be cleared that the same letters a, b, f, g will be also used for the cavity field coefficients in the frequency domain to avoid excessive use of symbols, and it is understood that these coefficients are different in both formulations in time and frequency domain.

Combining equations (3.5) through (3.7), upon substituting with the port fields, yields a matrix equation for the unknown amplitudes of the cavity eigenmodes and the port angular harmonics, of the form

$$[A]_{N\times N}[a]_{N\times 1} + [B]_{N\times M}\left[a^{scat}\right]_{M\times 1} = [C]_{N\times 1}\,. \tag{3.9}$$

The vectors $[a]_{N\times 1}$ and $[a^{scat}]_{M\times 1}$ hold as their elements the cavity and scattered electric field coefficients a_n and a_p^{scat}, respectively. Expressions for the matrix elements of $[A]$, $[B]$ and $[C]$ are found in Appendix C.

3.2.4 Boundary Conditions Between Cavity Modes and Port Modes

It is to be noted that for scattering problems the complete set of cavity eigenmodes can be used with the cavity walls either PE or PM, using the choice which simplifies the solution of the problem. Although the tangential field components of either the eigenmode electric or magnetic field is zero at the cavity wall, the port field of the same kind ($\mathscr{E}^{port}$ or $\mathscr{H}^{port}$) couples to the eigenmode field ($\mathscr{E}^{cav}$ or $\mathscr{H}^{cav}$) with non zero tangential component through surface integral representing surface current, as in (3.5-3.6) . In addition, the matching of the port and cavity mode fields is applied directly for the field type ($\mathscr{E}^{cav}$ or $\mathscr{H}^{cav}$) with non zero tangential components for the cavity eigenmodes. A system of equations is generated from application of tangential field matching by using mode orthogonality of the port angular harmonic modes, viz. for PM cavity:

$$\oint_{S_t} \hat{\mathbf{n}} \times \mathbf{E}^{port}(\mathbf{a}) \cdot \mathbf{h}_{p'}(\mathbf{a}) ds = \oint_{S_t} \hat{\mathbf{n}} \times \left(\sum_n a_n \mathbf{E}_n(\mathbf{a}) + \sum_\alpha f_\alpha \mathbf{F}_\alpha(\mathbf{a}) \right) \cdot \mathbf{h}_{p'}(\mathbf{a}) ds \tag{3.10}$$

and for PE cavity:

$$\oint_{S_t} \hat{\mathbf{n}} \times \mathbf{H}^{port}(\mathbf{a}) \cdot \mathbf{e}_{p'}(\mathbf{a}) ds = \oint_{S_t} \hat{\mathbf{n}} \times \left(\sum_n b_n \mathbf{H}_n(\mathbf{a}) + \sum_\lambda g_\lambda \mathbf{G}_\lambda(\mathbf{a}) \right) \cdot \mathbf{e}_{p'}(\mathbf{a}) ds \tag{3.11}$$

where $p' = 1, 2, \cdots, M$ and $\mathbf{h}_{p'}(\mathbf{r}) = \frac{-1}{j\omega\mu_0} \nabla \times \mathbf{e}_{p'}(\mathbf{r})$. Proof of equations (3.10) and (3.11) is given in Appendix D.

Depending on the boundary conditions of the fictitious cavity, (3.9) is combined with either (3.10) for PM or (3.11) and (3.8) for PE boundaries, respectively, to yield

$$\begin{aligned} \left([\Omega]_{N\times N} + [\Gamma(\omega)]_{N\times N} \right) [a]_{N\times 1} &= [\Upsilon(\omega)]_{N\times N}, \\ [\Omega]_{N\times N} &= [EE]_{N\times N} - [EF]_{N\times L} [FF]^{-1}_{L\times L} [EF]^T_{L\times N} \end{aligned} \tag{3.12}$$

where the elements of $[EE]$, $[EF]$, and $[FF]$ are the cavity eigenmode projections $\langle \mathbf{E}_n, \mathbf{E}_{n'} \rangle$, $\langle \mathbf{E}_n, \mathbf{F}_\alpha \rangle$ and $\langle \mathbf{F}_\alpha, \mathbf{F}_{\alpha'} \rangle$, respectively. It is obvious that all the elements of $[\Omega]$ are integrations of the cavity mode projections and are thus frequency independent, whereas the elements of $[\Gamma(\omega)]$ and $[\Upsilon(\omega)]$ contain the frequency-dependent (ka) argument of the used Hankel functions in $\mathbf{e}_p$ with $k = \omega\sqrt{\mu_0\varepsilon_0}$ as detailed also in Appendix C. It is worth mentioning that, in case of lossy dielectrics, the dielectric constant will be replaced by its complex version $\varepsilon_c(\mathbf{r}) = \varepsilon(\mathbf{r}) + \frac{\sigma(\mathbf{r})}{j\omega}$. The involved integrals, however, remain frequency independent since the frequency acts as a scaling factor only.

3.3 Obtaining the Solution Over a Wide Range of Frequencies

The solution of (3.12) requires the evaluation of the inverse $([\Omega]+[\Gamma(\omega)])^{-1}$, which is evaluated in light of the theorem in [20] as follows:

let $[\xi_1]=[\Omega]^{-1}$, $[\xi_{i+1}]=[\xi_i]-g_i\,[\xi_i]_{(:,i)}\,[\Gamma_i]_{(i,:)}\,[\xi_i]$, where $[\xi_i]_{(:,i)}$ is a column vector with its elements are the ith column of $[\xi_i]$ and $[\Gamma_i]_{(i,:)}$ is a row vector with its elements are the ith row of $[\Gamma_i]$, $g_i=1/\left(1+\mathrm{tr}([\xi_i]\,[\Gamma_i])\right)$, and $i=2,\ldots,N$. Then, the required inverse may be obtained using:

$$([\Omega]+[\Gamma(\omega)])^{-1}=[\xi_N]-g_N\,[\xi_N]\,[\Gamma_N]\,[\xi_N]\,. \tag{3.13}$$

It is important to notice that in the previous inversion scheme, the evaluation of $[\Omega]^{-1}$ is done only once at some reference frequency and is stored. For any other frequency, applying the previous procedure provides the inverse $([\Omega]+[\Gamma(\omega)])^{-1}$ with no further inversion. Moreover, the inversion scheme is performed in forward not recursive manner avoiding memory overloading resulting from recursion. Also, by inspecting the matrices in (3.12), it is found that the matrix $[\Omega]$ as mentioned before is frequency independent and thus it is evaluated only once, while matrices $[\Gamma(\omega)]$ and $[\Upsilon(\omega)]$ are partially evaluated at the different frequency points, only for the terms with the surface integral of the port modes, which end up in a closed analytical form by virtue of the orthogonality which reduces surface integrals to direct substitution in the field expression. The terms with volume integrals of the eigenmodes are frequency independent and are evaluated at one frequency point. This results in considerable time-saving when the response over a wideband frequency range is to be determined, in contrast to other frequency-domain techniques, where the solution process (matrix filling and inversion) is to be conducted for each frequency point. Alternatively, an iterative solver can be employed to further accelerate the inversion process upon getting the solution at a reference frequency point.

3.4 Analysis of Geomtry and Material Variations

Starting with some baseline scatterer configuration, it may be required to analyze certain modifications of the scatterer with the goal of conducting sensitivity analysis concerning scatterer shape variations or, alternatively, optimization of the scatterer shape. In the proposed EPT, for the same fictitious canonical cavity, the surface integrals of the port modes remain unchanged, corresponding again to considerable time-saving. Subsequently, only volume integrals of the eigenmode projections over the modified regions need to be evaluated numerically.

Making use of orthogonality properties in Sec. 2.2.2.2 the projections could be simplified to integral on the dielectric object rather than on the whole cavity volume. Considering the projections of the electric field solenoidal eigenmodes,

$$\begin{aligned}\langle \mathbf{E}_n, \mathbf{E}_{n'} \rangle_{\text{base}} &= \int_{V_t} \varepsilon(\mathbf{r}) \mathbf{E}_n \cdot \mathbf{E}_{n'} dv \\ &= \varepsilon_0 \int_{V_t} \mathbf{E}_n \cdot \mathbf{E}_{n'} dv + \int_{V_d} (\varepsilon_d(\mathbf{r}) - \varepsilon_0) \mathbf{E}_n \cdot \mathbf{E}_{n'} dv \\ &= \varepsilon_0 \delta_{nn'} + \int_{V_d} (\varepsilon_d(\mathbf{r}) - \varepsilon_0) \mathbf{E}_n \cdot \mathbf{E}_{n'} dv \end{aligned} \tag{3.14}$$

where V_t is the cavity volume and V_d the dielectric volume.

Applying this to all eigenmode projections the following relations could be obtained:

$$\begin{aligned}\langle \mathbf{E}_n, \mathbf{E}_{n'} \rangle_{\text{base}} &= \varepsilon_0 \delta_{nn'} + \int_{V_d} (\varepsilon_d(\mathbf{r}) - \varepsilon_0) \mathbf{E}_n \cdot \mathbf{E}_{n'} dv, \\ \langle \mathbf{F}_\alpha, \mathbf{F}_{\alpha'} \rangle_{\text{base}} &= \varepsilon_0 \delta_{\alpha\alpha'} + \int_{V_d} (\varepsilon_d(\mathbf{r}) - \varepsilon_0) \mathbf{F}_\alpha \cdot \mathbf{F}_{\alpha'} dv, \\ \langle \mathbf{E}_n, \mathbf{F}_{\alpha'} \rangle_{\text{base}} &= \int_{V_d} (\varepsilon_d(\mathbf{r}) - \varepsilon_0) \mathbf{E}_n \cdot \mathbf{F}_{\alpha'} dv. \end{aligned} \tag{3.15}$$

Then, the modified scatterer will have integrals in the form:

$$\begin{aligned}\langle \mathbf{E}_n, \mathbf{E}_{n'} \rangle_{\text{mod}} &= \langle \mathbf{E}_n, \mathbf{E}_{n'} \rangle_{\text{base}} + \int_{V_\delta} (\varepsilon_\delta(\mathbf{r}) - \varepsilon_{\text{base}}(\mathbf{r})) \mathbf{E}_n \cdot \mathbf{E}_{n'} dv, \\ \langle \mathbf{F}_\alpha, \mathbf{F}_{\alpha'} \rangle_{\text{mod}} &= \langle \mathbf{F}_\alpha, \mathbf{F}_{\alpha'} \rangle_{\text{base}} + \int_{V_\delta} (\varepsilon_\delta(\mathbf{r}) - \varepsilon_{\text{base}}(\mathbf{r})) \mathbf{F}_\alpha \cdot \mathbf{F}_{\alpha'} dv, \\ \langle \mathbf{E}_n, \mathbf{F}_{\alpha'} \rangle_{\text{mod}} &= \langle \mathbf{E}_n, \mathbf{F}_{\alpha'} \rangle_{\text{base}} + \int_{V_\delta} (\varepsilon_\delta(\mathbf{r}) - \varepsilon_{\text{base}}(\mathbf{r})) \mathbf{E}_n \cdot \mathbf{F}_{\alpha'} dv \end{aligned} \tag{3.16}$$

where V_δ is the added/subtracted volume, $\varepsilon_\delta(\mathbf{r})$ the new dielectric constant within V_δ, and $\varepsilon_{\text{base}}(\mathbf{r})$ the dielectric constant within the same volume before the modification, as illustrated in Fig. 3.2.

It should be mentioned that there is no constraint on the modification size as long as the canonical cavity is maintained. Moreover for the case of changing the dielectric constant of a given scatterer homogeneously, no integrations will be evaluated at all and the integrals over V_d in (3.15) will be simply scaled by the ratio of $\left(\varepsilon_{d,new} - \varepsilon_0\right) / \left(\varepsilon_{d,base} - \varepsilon_0\right)$.

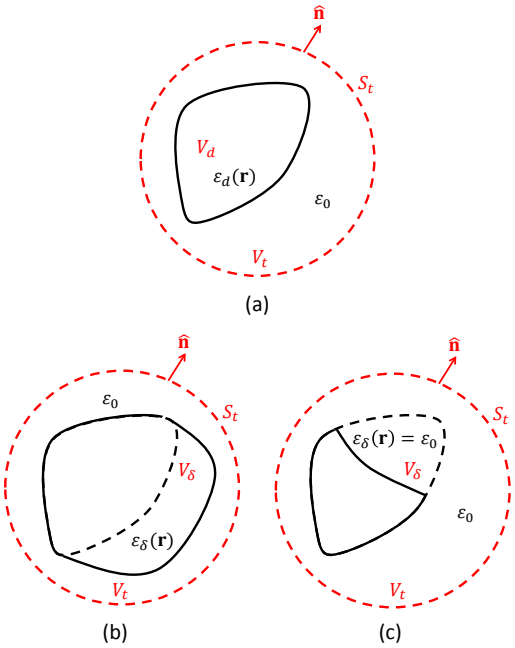

Figure 3.2: Illustration of possible modifications to a scatterer: (a) baseline object, (b) modified object by adding volume, and (c) modified object by subtracting volume.

3.5 Results

Bistatic scattering width (SW), normalized to free space wavelength (λ) of 2D dielectric objects is used to verify the proposed technique. In Fig. 3.3, results obtained for a circular cylindrical dielectric scatterer illuminated by transverse electric TE^z plane wave using the EPT solution in Appendix A.4 are compared with the analytical solution in [21], showing the convergence of the solution as the number of modes increases. As a rule of thumb, the number of eigenmodes required to reach convergence are $N, L, O = \lceil 8k_d a \rceil$ with k_d being the wave number of the dielectric material at the operating frequency.

In Appendix A, it will be shown that the solution for Helmholtz equations for the circular cavity eigenmodes will be in the form of angular harmonics with eigenvalues that are directly related to either the zeros of Bessel function or its derivative for different orders. The adopted numbering scheme is by sorting the eigenvalues in ascending order and then use the required number of eigenmodes according to the rule of thumb.

In Fig. 3.4, results are obtained for circular cylindrical scatterer excited by an electric line source for two cases: the first with the line source outside the canonical cavity, and the second with the line source inside the canonical cavity (thus taken into consideration in (3.6)) following the solutions provided in Appendices A.2 and A.2 , respectively. The results illustrate that the two solutions converge to the analytical solution provided in [21].

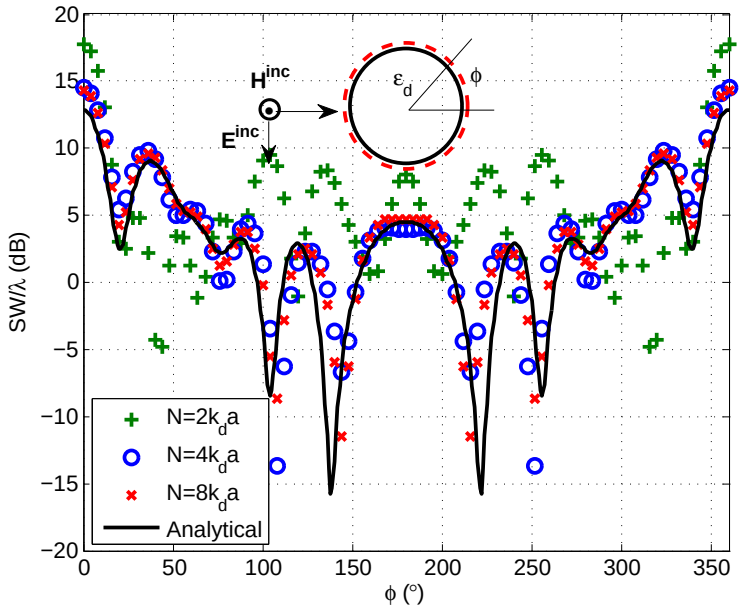

Figure 3.3: SW for cylindrical dielectric scatterer with $\varepsilon_d = 4\varepsilon_0$ and radius = λ illuminated by TE^z plane wave with the canonical cavity touching the dielectric surface.

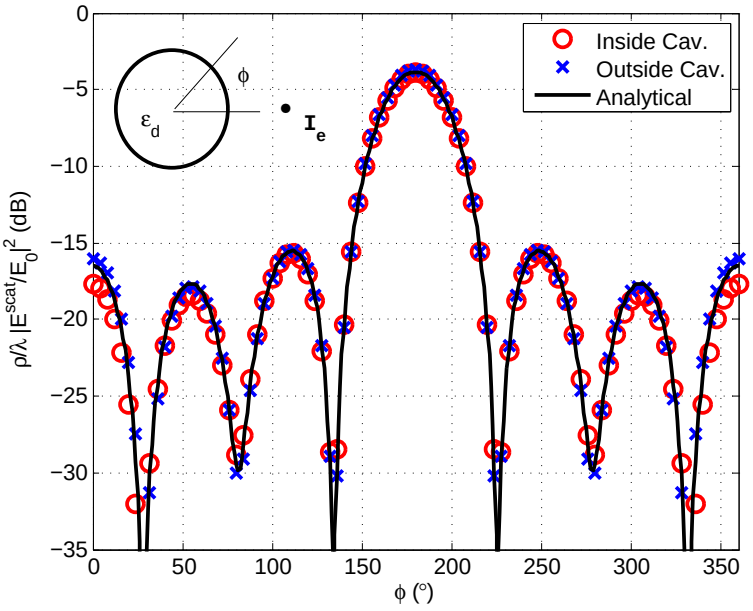

Figure 3.4: Scattered field from cylindrical dielectric scatterer with $\varepsilon_d = 3\varepsilon_0$ and radius = 0.5λ illuminated by electric line source having $E_0 = -I_e\frac{\omega\mu_0}{4}$ located at distance λ from the dielectric scatterer center. The radius of the canonical cavity is $a = 0.5\lambda$ (I_e outside the cavity) and $a = 1.2\lambda$ (I_e inside the cavity).

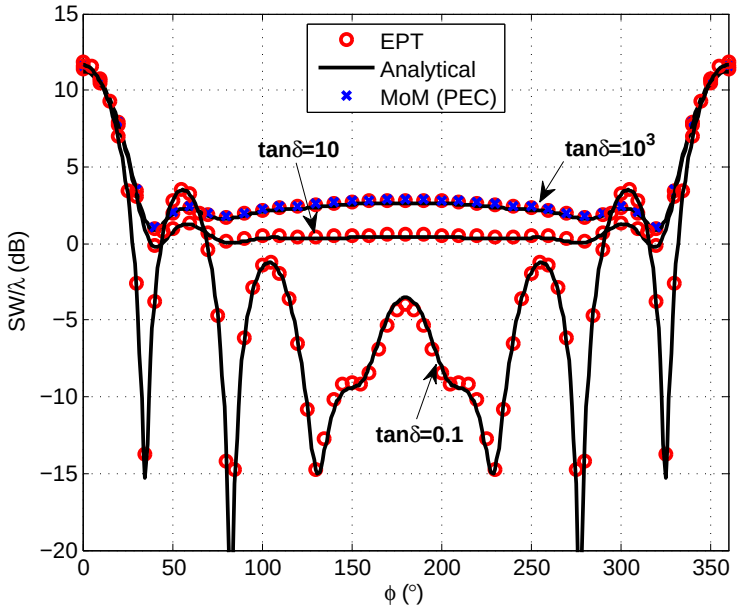

Figure 3.5: Scattered field from cylindrical dielectric scatterer with real dielectric constant of $3\varepsilon_0$, variable loss tangent, and radius = 0.6λ illuminated by TM^z plane wave with the canonical cavity touching the dielectric surface.

Fig. 3.5 shows the results for the case of lossy dielectric by using a complex dielectric constant in the formulation. The results in Fig. 3.5 are obtained for cylindrical scatterer excited by TM^z plane wave for different loss tangents. The results illustrate that the solutions converge to the analytical solution provided in [21]. Also, for high loss tangent the results are in very good agreement with those obtained using the MoM a for PEC cylinder, which validates the modeling of perfecting conducting objects using high conductivity material in the EPT.

In the proposed approach making use of the frequency independent feature of the generated matrices and filling it only once, allows studying the frequency dependent scattering by the object with the number of modes taken according to the maximum frequency as in Fig. 3.6. The results obtained for circular cylindrical scatterer, for the forward scattering width, are compared with the analytical solution in [21] with the number of eigenmodes set to $\lceil 8k_{d,max}a \rceil$.

To make a comparison between direct solution, i.e., solving at each frequency point with the corresponding number of modes, and the frequency independent matrix approach, a speed-up factor is defined as:

$$\text{Speed-up Factor} = \frac{\text{Time for direct approach}}{\text{Time for accelerated approach}} \tag{3.17}$$

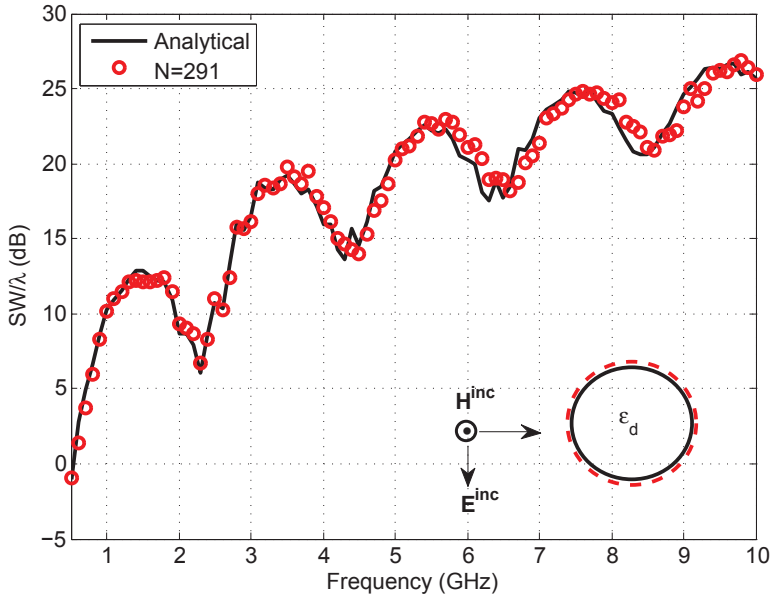

Figure 3.6: Forward SW for cylindrical dielectric scatterer with $\varepsilon_d = 3\varepsilon_0$ and radius = 0.1 m illuminated by TE^z plane wave with canonical cavity touching the dielectric surface.

Fig. 3.7 shows the speed-up factor for the cylindrical scatterer studied in Fig. 3.6. The number of modes utilized in the direct approach is $\lceil 8k_d a \rceil$ for each frequency points with all the matrices calculated, while the accelerated technique utilizes $\lceil 8k_{d,max} a \rceil$ for all frequency points with the frequency independent matrices calculated only once. This speed-up factor accounts for comparison in filling time only, with the matrix inversion conducted using direct inversion techniques, i.e., without using the approach in (3.13). It is worth noting that the speed-up factor increases as the number of frequency points increases due to the reduction in the matrix filling time, even with the direct approach using less number of modes for lower frequencies. Even at a wide range of frequencies (larger maximum to minimum frequency ratio f_{max}/f_{min}, the speed-up factor is still greater than unity with a monotonic increase as the number of sampled frequencies increase.

Fig. 3.8 provides another case for verification by considering a rectangular dielectric scatterer illuminated by transverse magnetic TM^z plane wave using the EPT solution in Appendix A.1. Results are compared with those of the MoM and exhibit very good agreement.

The approach for solving a modification of a baseline scatterer is verified by considering the case in Fig. 3.9, which shows baseline dielectric object in Fig. 3.9(a) and then the solution is obtained for the modified object in Fig. 3.9(b) making use of the previous solution with the involved integrations evaluated only for the added area. The results are compared with the MoM solution in Fig. 3.10.

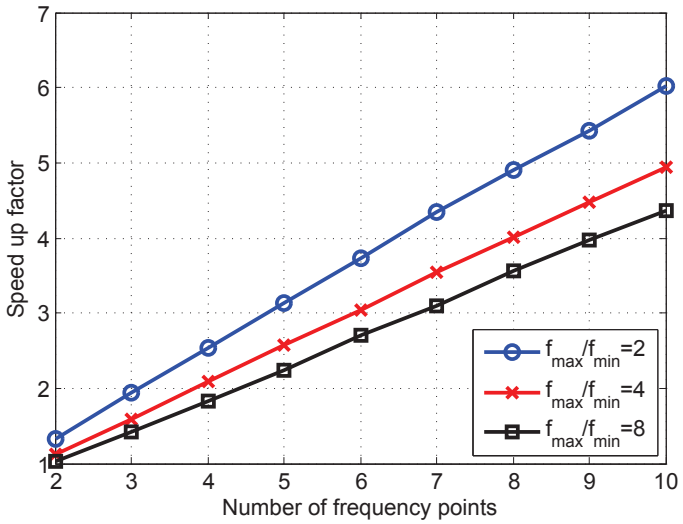

Figure 3.7: Speed-up factor for cylindrical dielectric scatterer with $\varepsilon_d = 3\varepsilon_0$ and radius = 0.1 m illuminated by TE^z plane wave with an equal-sized cylindrical cavity at different maximum-to-minimum frequency ratios, $f_{min} = 1$ GHz.

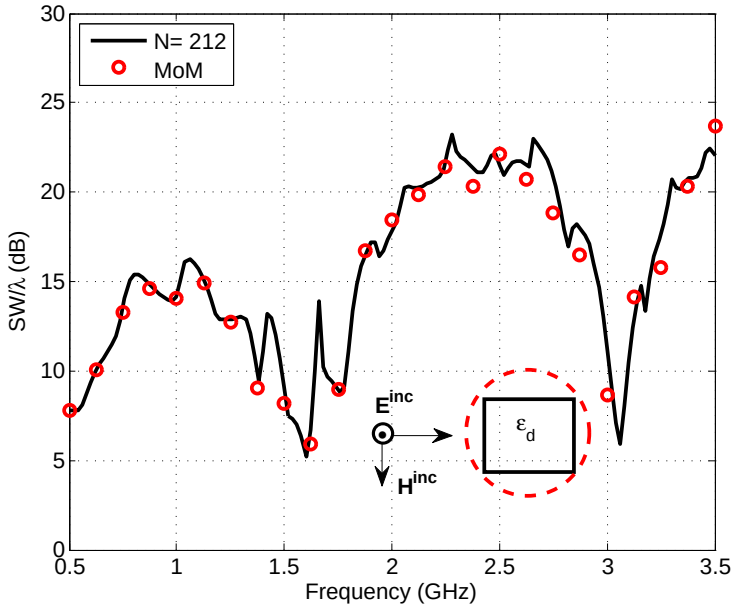

Figure 3.8: Forward SW for rectangular dielectric scatterer with $\varepsilon_d = 4\varepsilon_0$ and dimensions $0.2 \times 0.3\,\mathrm{m}^2$ illuminated by TM^z plane wave incident perpendicular to its long side with a circumscribing circular cylinder compared with the results obtained using MoM.

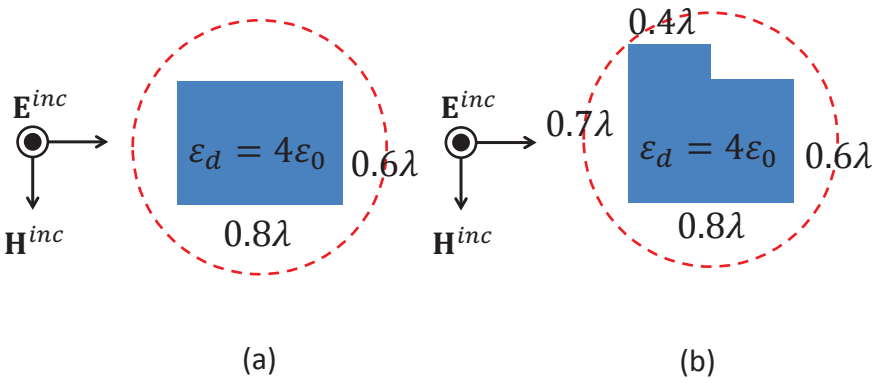

Figure 3.9: (a) Baseline dielectric rectangular scatterer (b) Perturbed dielectric scatterer. The cavity has radius=0.5315λ.

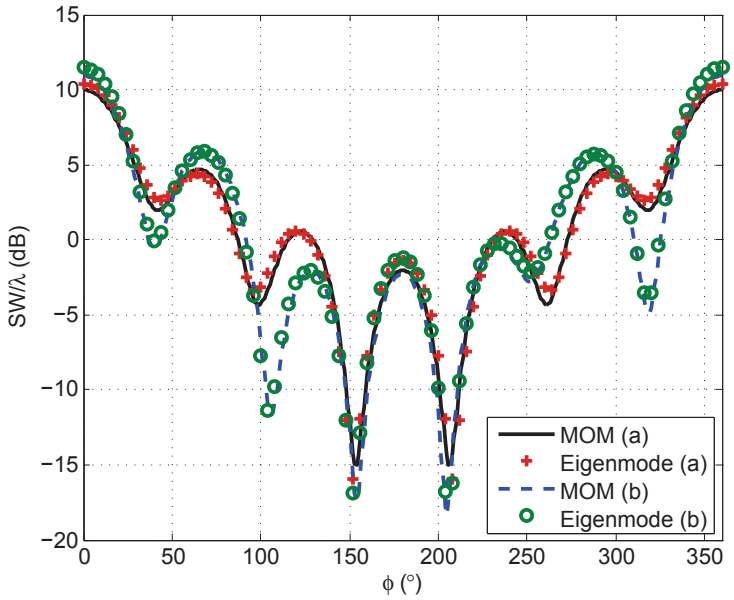

Figure 3.10: Results for eigenmode projection technique compared with the MoM solution for Fig. 3.9.

It should be noted that to have the benefit of fast perturbation analysis, all shape variations should be kept within the canonical cavity thus it must be chosen large enough to fit the shape variations. It should not be excessively large, however, to avoid large number of needed eigenmodes to solve the problem.

Fig. 3.11 shows another illustration example where the solution is obtained for the dielectric object in Figure 3.11(a) and then it is required for the dielectric shell in Fig. 3.11(b) making use of the first solution with the encountered numerical integrations evaluated only for the subtracted area. The speed up of the solution is shown in Fig. 3.12 for variable inner radius.

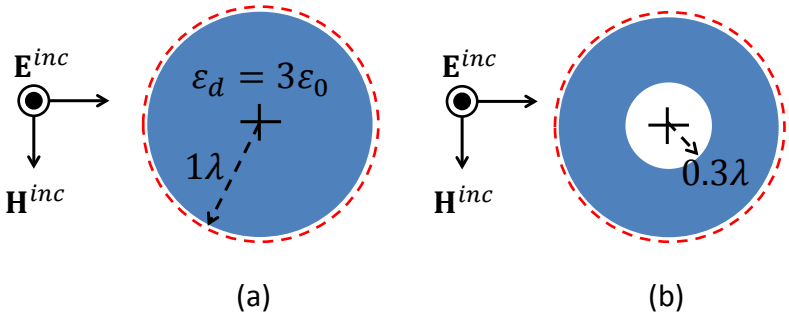

Figure 3.11: (a) Original dielectric cylindrical scatterer (b) Dielectric shell.

In Fig. 3.13 the solution of a cylindrical object is obtained in two cases with a dielectric constant of $3\varepsilon_0$ and $9\varepsilon_0$. The solution of the latter case obtained with no integrations evaluation at all and only matrices scaling by a factor of 4 is needed.

To make a comparison between the solution computational resources and accuracy of the EPT and the MoM, the example illustrated in Fig. 3.9(a) is considered using a canonical cavity of radius $a = 0.5\lambda$. First, comparing the size of matrices, the EPT matrix size is $\lceil 8k_d a \rceil^2$ whereas the MoM matrix size, assuming 20 unknowns per wavelength, for electric and magnetic currents will be $\lceil 2 \times 20 \times \text{perimeter in } \lambda \times \sqrt{\varepsilon_r} \rceil^2$. For the specific example under consideration, the MoM matrix is almost 20 times larger! For 3D problems, this ratio is expected to be significantly increased. This result illustrates a very considerable advantage of the EPT over the MoM, for having much smaller matrix size. Next, comparing the matrix condition number of both techniques, the MoM matrix has a condition number of 6.7013×10^5, compared to only 150.7927 for the EPT. Finally, and as already mentioned, the EPT has automatic and natural choice of the basis functions, i.e. the eigenmodes, and no singular integrals, thus no singularity extraction problems. The latter issues are all inherent problems in the MoM, in addition to the frequency-dependent nature of the MoM matrix due to the use of the Green's function, and the inability to handle perturbations in the object under consideration in an easy

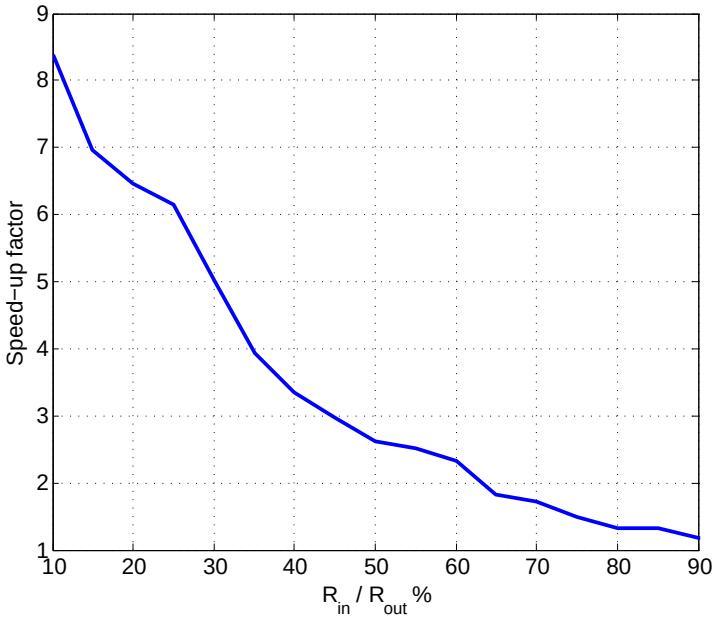

Figure 3.12: Speed-up factor for a cylindrical shell with $\varepsilon_d = 3\varepsilon_0$ and outer radius (R_{out}) = λ illuminated by TM^z plane wave with an equal-sized cylindrical cavity.

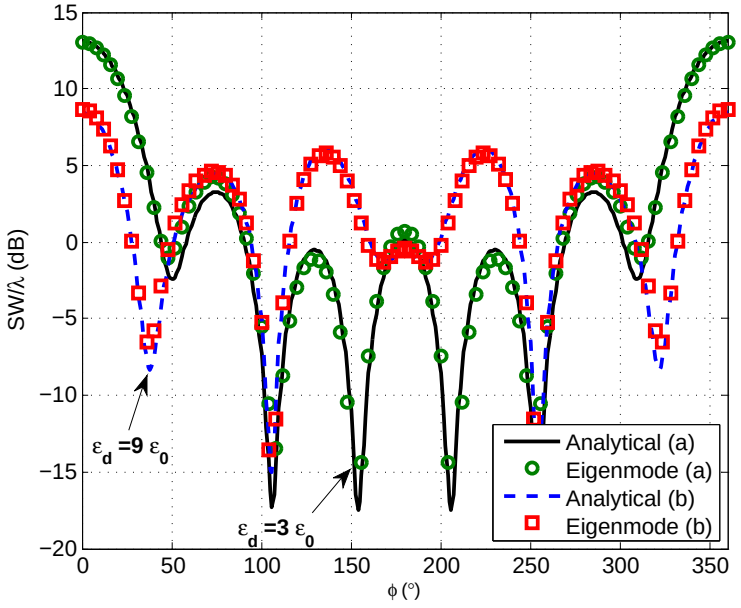

Figure 3.13: SW for cylindrical dielectric scatterer with (a)$\varepsilon_d = 3\varepsilon_0$, (b) $\varepsilon_d = 9\varepsilon_0$ and radius = 0.5λ illuminated by TM^z plane wave with canonical cavity touching the dielectric surface.

manner. The numerical integrals are performed with resolution resulting convergence of the integral.

Chapter 4

Electromagnetic Cavity Resonance Analysis Using the Eigenmode Projection Technique

RESONANCE of arbitrary-shaped cavities is analyzed in this chapter using the EPT, where a new approach is introduced with direct and efficient spurious modes separation by modeling the cavity walls by a highly conductive material. First, the general derivation is introduced, then results for canonical and arbitrary-shaped cavities are verified using analytical formulas and CST commercial simulation package solution.

4.1 General Problem Formulation

In [14] the eigenmode expansion was utilized in the solution of arbitrary-shaped cavities. The problem was defined as an arbitrarily-shaped, vacuum PEC cavity of volume V, with canonical expansion modes defined over the canonical fictitious cavity enclosure domain of volume V_t, as depicted in Fig. 4.1. The reminiscent volume of the domain δV is considered as if it is filled with PEC. Using the surface equivalence principle, the PEC is then replaced by a current on the arbitrary-cavity surface. This current is expressed in terms of the canonical cavity magnetic field expansion. However, the resulting eigenvalues were differentiated into two sets. The first set is the physical modes inside V, where the eigenvalue and the eigenvector corresponds to a natural resonance mode. The other set is the fake (spurious) modes which

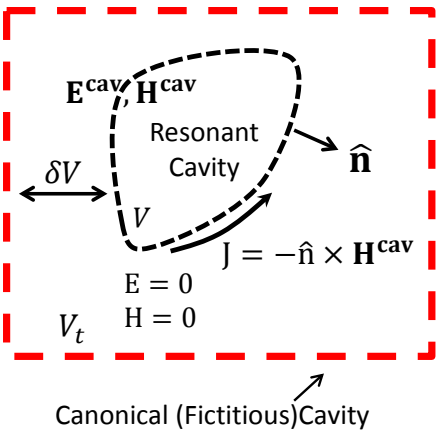

Figure 4.1: Arbitrary-shaped PEC cavity. The geometry of the problem can be interpreted as a canonical cavity containing PEC.

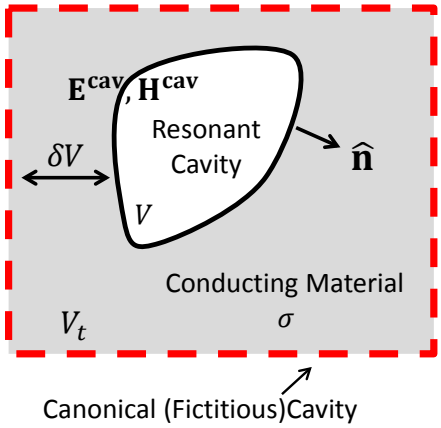

Figure 4.2: Arbitrary-shaped cavity. The geometry of the problem can be interpreted as a canonical cavity containing conducting material.

have zero total energy inside V and near zero eigenvalues. These spurious modes required exhaustive post processing for separation and this may not be successful in all cases.

The new proposed approach depends on replacing the PEC by a conducting material as illustrated in Fig. 4.2. This will result in complex eigenvalues (resonance frequencies) and the spurious modes will be directly separated by comparing the real and imaginary parts of the eigenvalue of the resulted modes.

The difference between resonance and scattering problems is that in resonance problems the structure is closed with no ports or interfaces. The solution of the problem using the eigenmode projections will be obtained using equations (2.23-2.26). The equations will be casted to the problem as follows: first, the surface integrals that represent the coupling between outer modes and canonical cavity eigenmodes vanish due to the fact that this is a closed problems and there is no outer modes; second, there is no mode matching at the boundaries because this is a closed problem. Considering homogeneous conducting material the equations will be as follows in frequency domain:

$$k_n a_n = -j\omega\mu_0 b_n \tag{4.1}$$
$$k_n b_n = j\omega\varepsilon_0 a_n + \sigma \langle \mathbf{E}_n, \mathbf{E}_{n'} \rangle a_n + \sigma \langle \mathbf{E}_n, \mathbf{F}_\alpha \rangle f_\alpha \tag{4.2}$$
$$g_\lambda = 0 \tag{4.3}$$

where $\langle \mathbf{E}_n, \mathbf{E}_{n'} \rangle$ and $\langle \mathbf{E}_n, \mathbf{F}_\alpha \rangle$ represents cavity eigenmode projections.

$$\langle \mathbf{E}_n, \mathbf{E}_{n'} \rangle = \int_{\delta V} \mathbf{E}_n(\mathbf{r}) \cdot \mathbf{E}_{n'}(\mathbf{r}) dv \tag{4.4}$$
$$\langle \mathbf{E}_n, \mathbf{F}_\alpha \rangle = \int_{\delta V} \mathbf{E}_n(\mathbf{r}) \cdot \mathbf{F}_\alpha(\mathbf{r}) dv \tag{4.5}$$

However, (2.25) will be descarded and the divergence equation (2.17) will be reformulated considering the conducting material and making use of the continuity equation. The electric charge density ρ_e could result from either an impressed charge or the existence of a lossy conducting material which is the case in our problem. In this case, ρ_e could be obtained from the continuity equation as follows

$$\nabla \cdot \mathbf{J} = -j\omega\rho_e \tag{4.6}$$

where $\mathbf{J}$ in our problem is the conduction current and could be expressed in terms of the electric field as $\mathbf{J} = \sigma\mathbf{E}$ with $\mathbf{E} = \frac{1}{\varepsilon_0}\mathbf{D}$. Substituting in the continuity equation, the equation will be as follows

$$\rho_e = \frac{-\sigma}{j\omega\varepsilon_0} \nabla \cdot \mathbf{D} = j\tan\delta \, (\nabla \cdot \mathbf{D}) \tag{4.7}$$

where $\tan\delta$ is the loss tangent of the conducting material.

$$\tan\delta = \begin{cases} 0 & \text{inside cavity vaccum} \\ \tan\delta_c & \text{inside conductor} \end{cases} \tag{4.8}$$

Substituting from (4.7) into (2.17)

$$\nabla \cdot (\mathbf{D} - j\tan\delta\mathbf{D}) = 0 \tag{4.9}$$

Considering homogeneous dielectric constant the equation could be represented in terms of electric field as follows

$$\nabla \cdot (\mathbf{E} - j\tan\delta\mathbf{E}) = 0 \tag{4.10}$$

Following similar procedure as in Sec. 2.2.3 by projecting the previous equation on ϕ_α, also the mathematical identity $\nabla \cdot (\phi \mathbf{A}) = \mathbf{A} \cdot \nabla\phi + \phi \nabla \cdot \mathbf{A}$ will be used as follows

$$\int_{\delta V} \nabla \cdot (\mathbf{E} - j\tan\delta \mathbf{E})\, \phi_\alpha dv = 0$$

$$\int_{\delta V} \nabla \cdot ((\mathbf{E} - j\tan\delta \mathbf{E})\, \phi_\alpha)\, dv - \int_{\delta V} (\mathbf{E} - j\tan\delta \mathbf{E})\, \nabla\phi_\alpha dv = 0 \tag{4.11}$$

Applying the divergence theorem, the integral in the left will be converted into a surface integral which vanishes due to the fact that this is a closed problem and the fields vanish at the boundaries. Substituting with the field expansion and making use of orthogonality in (2.10), equation (4.11) will be in the following form

$$f_\alpha - j\tan\delta_c \left[\sum_n a_n \langle \mathbf{E}_n, \mathbf{F}_\alpha \rangle + \sum_{\alpha'} f_{\alpha'} \langle \mathbf{F}_\alpha, \mathbf{F}_{\alpha'} \rangle \right] = 0 \tag{4.12}$$

with,

$$\langle \mathbf{F}_\alpha, \mathbf{F}_{\alpha'} \rangle = \int_{\delta V} \mathbf{F}_\alpha(\mathbf{r}) \cdot \mathbf{F}_{\alpha'}(\mathbf{r}) dv \tag{4.13}$$

Casting (4.12) in matrix form,

$$[f] = [Z]\,[a]\,,\ [Z] = [\mathrm{I} - j\tan\delta_c\,[FF]]^{-1}\, j\tan\delta_c\,[EF]^T \tag{4.14}$$

where I is an identity matrix, the matrix $[FF]$ and $[EF]$ hold as their elements the cavity eigenmode projections $\langle \mathbf{F}_\alpha, \mathbf{F}_{\alpha'} \rangle$ and $\langle \mathbf{E}_n, \mathbf{F}_\alpha \rangle$, respectively.

Substituting form (4.14) in (4.2) results in the following equation, in matrix form

$$\mathrm{diag}(k_n)\,[b] = j\omega\varepsilon_0\,[a] + \sigma\,[EE]\,[a] + \sigma\,[EF]\,[\mathbf{Z}]\,[a] \tag{4.15}$$

where $\mathrm{diag}(k_n)$ is a diagonal matrix with its elements are k_n and $[EE]$ hold as its elements the cavity eigenmode projections $\langle \mathbf{E}_n, \mathbf{E}_{n'} \rangle$.

Rewriting the system of equations and substituting from (4.1) into (4.15) and doing some simplification,

$$-\frac{1}{j\omega\mu_0}\text{diag}(k_n^2)\,[a] = j\omega\varepsilon_0\left(\mathrm{I} - j\tan\delta_c\,[EE] - j\tan\delta_c\,[EF]\,[\mathbf{Z}]\right)[a] \tag{4.16}$$

$$k_n^2\,[a] = k^2\left(\mathrm{I} - j\tan\delta_c\,[EE] - j\tan\delta_c\,[EF]\,[\mathbf{Z}]\right)[a] \tag{4.17}$$

$$\frac{1}{k^2}\,[a] = \frac{1}{k_n^2}\left(\mathrm{I} - j\tan\delta_c\,[EE_{nm}] - j\tan\delta_c\,[EF_{n\alpha}]\,[\mathbf{Z}]\right)[a] \tag{4.18}$$

(4.18) represents an eigenvalue problem with the eigenvalues are $\frac{1}{k^2}$. It should be noted that to obtain the resonance problem for PEC cavity, the conductivity σ should be chosen with high value. Thus assuming that the loss tangent $\tan\delta_c$ is constant with a high value will give good results and simplify the solution of the problem at the same time.

In the next section, the proposed solution will be used to obtain the resonance frequencies of the cavities used in linear accelerators (LINAC) where determination of the resonance frequencies is necessary to optimize the design. The cavities used in LINAC are body of revolution cavities (BOR). Assuming that the electron beam is confined at the axis of the cavity, then there is no need to consider the modes with azimuthal variations as the electron beam will excite only modes with no azimuthal variations.

4.2 Body of Revolution Cavities with no Azimuthal Variations

The general problem under investigation is illustrated in Fig. 4.3. It is straight forward that the most appropriate choice of the canonical cavity in this problem is a finite-lenght circular cylinder with PEC walls. The cylinder radius (a) and length d are chosen such that it completely enclose the cavity. In this work, the solution is obtained for TM^z arbitrary cavity modes and the canonical cavity solenoidal and irrotational eigenmodes will be derived in the following sections.

4.2.1 Solenoidal Eigenmodes

Expanding the two curl equations in (2.7) with $\frac{\partial}{\partial\phi} = 0$ leads to the following equations:

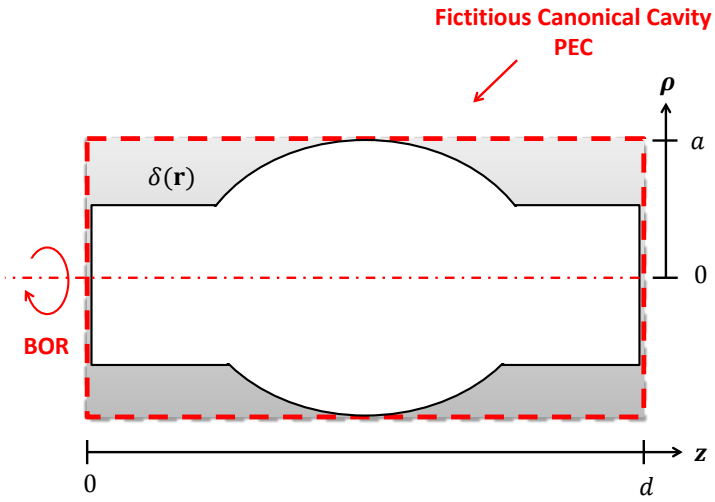

Figure 4.3: BOR cavity enclosed by cylindrical canonical cavity.

$$k_n E_{n\rho} = -\frac{\partial H_{n\phi}}{\partial z} \tag{4.19}$$

$$k_n E_{n\phi} = \frac{\partial H_{n\rho}}{\partial z} - \frac{\partial H_{nz}}{\partial \rho} \tag{4.20}$$

$$k_n E_{nz} = \frac{1}{\rho}\frac{\partial}{\partial \rho}\left(\rho H_{n\phi}\right) \tag{4.21}$$

$$k_n H_{n\rho} = -\frac{\partial E_{n\phi}}{\partial z} \tag{4.22}$$

$$k_n H_{n\phi} = \frac{\partial E_{n\rho}}{\partial z} - \frac{\partial E_{nz}}{\partial \rho} \tag{4.23}$$

$$k_n H_{nz} = \frac{1}{\rho}\frac{\partial}{\partial \rho}\left(\rho E_{n\phi}\right) \tag{4.24}$$

It could be noted that the system of equations could be separated to two parts as follows: equations (4.19), (4.21) and (4.23) represents TM^z modes and the rest of the equations represents TE^z modes. Considering TM^z modes then equations (4.19), (4.21) and (4.23) are the system of equations to be solved.

First of all, E_{nz} is obtained by solving 2.4 for PE boundary, using ∇^2 expression in [22, P. 919],

$$\left(\frac{\partial^2}{\partial \rho^2} + \frac{1}{\rho}\frac{\partial}{\partial \rho} + \frac{\partial^2}{\partial z^2} + k_n^2\right) E_{nz} = 0 \tag{4.25}$$

Using separation of variables and substituting by $E_{nz} = E_\rho(\rho)E_z(z)$ then (4.25) could be written as follows:

$$\frac{1}{E_\rho(\rho)}\frac{\partial^2 E_\rho(\rho)}{\partial\rho^2} + \frac{1}{E_\rho(\rho)}\frac{1}{\rho}\frac{\partial E_\rho(\rho)}{\partial\rho} + k_n^2 = -\frac{1}{E_z(z)}\frac{\partial^2 E_z(z)}{\partial z^2} = k_z^2 \tag{4.26}$$

Two separate differential equations are obtained from the previous equation,

$$\rho^2\frac{\partial^2 E_\rho(\rho)}{\partial\rho^2} + \rho\frac{\partial E_\rho(\rho)}{\partial\rho} + \rho^2\left(k_n^2 - k_z^2\right)E_\rho(\rho) = 0 \tag{4.27}$$

$$\frac{\partial^2 E_z(z)}{\partial z^2} + k_z^2 E_z(z) = 0 \tag{4.28}$$

Let $k_c^2 = k_n^2 - k_z^2$ then the solution of (4.27) will be in the form

$$E_\rho(\rho) = AJ_0(k_c\rho) + BY_0(k_c\rho) \tag{4.29}$$

and since the function $Y_0(k_c\rho)$ is singular at $\rho = 0$ then $B = 0$, while the solution of (4.28) will be in the form

$$E_z(z) = Ccos(k_z z) + Dsin(k_z z) \tag{4.30}$$

For PE boundary at z=0, only the cosine variation will considered,

$$E_{nz} = E_n J_0(k_c\rho)cos(k_z z) \tag{4.31}$$

where E_n is the magnitude of cavity modes solenoidal electric field which is obtained such that the fields are normalized with respect to the volume integral of the self terms i.e. $\int_{V_t} E_n.E_n ds = 1$.

Now after E_{nz} is obtained, the other field components will be driven using its expression. First, (4.31) is substituted into (4.23) resulting in (4.32),

$$H_{n\phi} = -\frac{k_n}{k_c}E_n J_0^{'}(k_c\rho)cos(k_z z) \tag{4.32}$$

then (4.32)is substituted into (4.19) resulting in (4.33).

$$E_{n\rho} = -\frac{k_z}{k_c} E_n J_0^{'}(k_c\rho) sin(k_z z) \tag{4.33}$$

Applying the boundary conditions at the cavity surfaces ($E_{nz} = 0$ at $\rho = a$ and $E_{n\rho} = 0$ at $z = 0, d$) then:

$$\begin{aligned} k_c &= \frac{P_{0n_1}}{a} \\ k_z &= \frac{n_2\pi}{d} \\ k_n^2 &= \left(\frac{P_{0n_1}}{a}\right)^2 + \left(\frac{n_2\pi}{d}\right)^2 \end{aligned} \tag{4.34}$$

where P_{0m} is the m^{th} root of J_0. From previous, the total solenoidal electric field could be expressed as follows:

$$\mathbf{E}_n = -\frac{k_z}{k_c} E_n J_0^{'}(k_c\rho) sin(k_z z) a_\rho + E_n J_0(k_c\rho) cos(k_z z) a_z \tag{4.35}$$

4.2.2 Irrotational Eigenmodes

Solving 2.5 with PE boundary at the cavity surface ($\phi_\alpha = 0$ at $\rho = a$ and at $z = 0, d$). The result could be expressed as follows

$$\begin{aligned} \phi_\alpha &= U_\alpha J_0(l_{\alpha_1}\rho) sin(l_{\alpha_2} z) \\ F_\alpha &= \frac{l_{\alpha_1}}{l_\alpha} U_\alpha J_0^{'}(l_{\alpha_1}\rho) sin(l_{\alpha_2} z) a_\rho + \frac{l_{\alpha_2}}{l_\alpha} U_\alpha J_0(l_{\alpha_1}\rho) cos(l_{\alpha_2} z) a_z \end{aligned} \tag{4.36}$$

where U_α is the magnitude of the electric scalar potential which is obtained such that the normalization identity $\int_{V_t} U_\alpha U_\alpha ds = 1$ is satisfied with

$$\begin{aligned} l_{\alpha_1} &= \frac{P_{0\alpha_1}}{a} \\ l_{\alpha_2} &= \frac{\alpha_2\pi}{d} \\ l_\alpha^2 &= \left(\frac{P_{0\alpha_1}}{a}\right)^2 + \left(\frac{\alpha_2\pi}{d}\right)^2 \end{aligned} \tag{4.37}$$

The field eigenmodes expressions are now ready to be used in the solution of the problem under investigation. In the next section, results for canonical and arbitrary-shaped BOR cavities with no azimuthal variations are verified using analytical formulas for circular canonical cavities and CST commercial simulation package for arbitrary-shaped cavities.

4.3 Results

4.3.1 Verification with Canonical Case

First, the technique is verified for circular cylindrical cavity as illustrated in Fig. 4.4. The solution of circular cavity of radius b is obtained using the eigenmodes of another circular fictitious canonical cavity of radius a, where $a > b$.

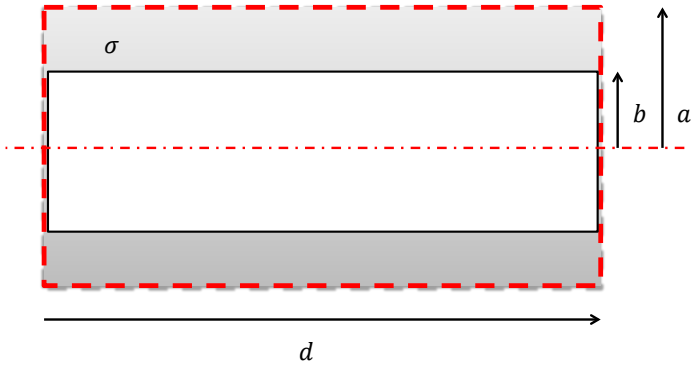

Figure 4.4: cylindrical cavity enclosed by cylindrical canonical cavity.

Fig. 4.5 shows the results of the complex propagation constant for cylindrical cavity or radius $b = 1.5$ cm using the eigenmode expansion provided by another canonical cavity with larger radius of $a = 2$ cm using 30 eigenmodes.

It is obvious from the results that the eigenvalues are directly separated into two sets: modes resonating in the conductor and modes resonating inside the cavity.

The first set is equivalent to spurious modes in the solution approach proposed in [14], while the second set represents the actual required modes.

In this work, the separation of the modes is straight forward by comparing the real and imaginary parts of the complex propagation constant. The actual modes are the modes with high real part compared to the imaginary part (10 times larger) for high value of conductivity.

The effect of conductivity is illustrated in Table 4.1 for the first resonance with the same number of modes at different values of the loss tangent. It is obvious that for the same number of eigenmodes the resonance frequencies is more accurate for higher conductivity.

Table (4.2) shows the effect of the number of used eigenmodes on the solution accuracy, illustrating that increasing the number of eigenmodes decreases the solution error.

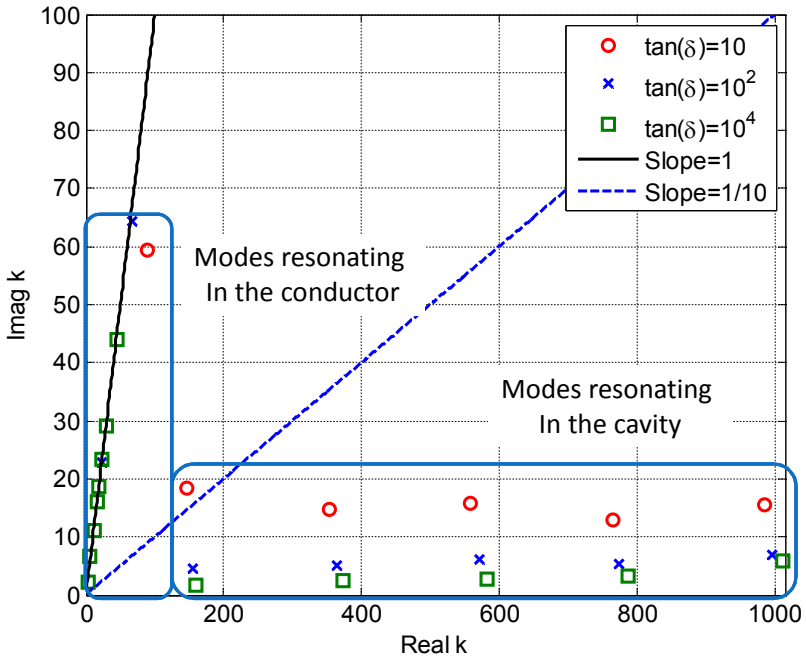

Figure 4.5: Complex propagation constant for cylindrical case with b=1.5, a=2 cm.

	Theoretical	$\tan\delta_c = 10$	$\tan\delta_c = 10^2$	$\tan\delta_c = 10^4$
Resonance Frequency	7.6394 GHz	6.9567 GHz	7.4294 GHz	7.6633 GHz
Relative Error %		8.937 %	2.7489 %	0.3128 %

Table 4.1: The effect of conductivity on cavity eigenmodes

The eigenvalue problem results also in the eigenvectors which represents the field coefficients of the eigenmode expansion for each resonance. Figures 4.6, 4.7, and 4.8 illustrates the field plot inside the cavity using the eigenvectors (coefficients) of TM_{01}, TM_{02}, and TM_{03} modes with very good agreement with the analytical formula.

Fig. 4.9 shows another result of the complex propagation constant for cylindrical cavity or radius $b = 1$ cm. The canonical cavity radius equals $a = 2$ cm and the number of modes used equals to 100 with a filling material of $\tan(\delta) = 10^4$. Also, the plot for TM_{01} is illustrated in Fig. 4.10 compared with the theoretical formula.

4.3.2 Verification with Arbitrary Shape

Second, the problem of stepped cavity illustrated in Fig. 4.11 is used as a sample arbitrary-shaped BOR cavity and it is verified using CST commercial solver. The complex eigenvalues of stepped cavity with dimensions $a = 1.5, b = 2, d_{in} = 3.5$ and $d = 10$ cm are illustrated in Fig. 4.12 with the separation of spurious modes still straight forward.

Table 4.3 illustrates the relative error between the resonance frequencies obtained by the CST and those of the EPT with 100 eigenmodes. It is obvious that there is a very good matching exists between the results.

	Relative Error %
N=30	0.3128
N=60	0.0307
N=120	0.0194

Table 4.2: The effect of number of eigenmodes on solution accuracy for loss tangent $\tan\delta_c = 10^4$.

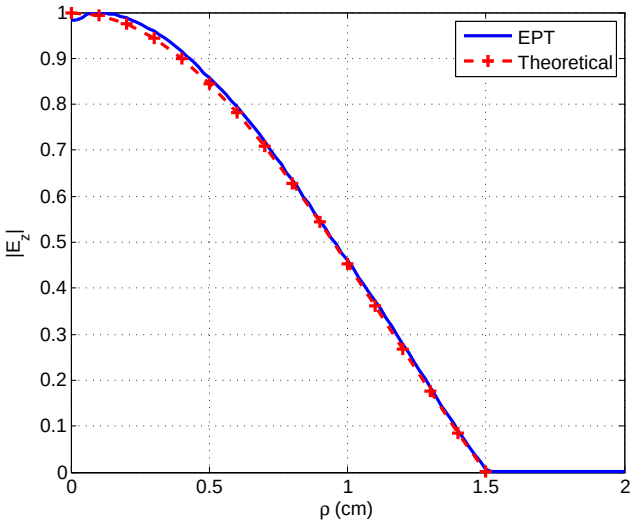

Figure 4.6: Field plot versus radial distance for TM_{01} mode of cavity of radius b=1.5 enclosed by canonical cavity of radius a=2 cm.

Figures 4.13, 4.14, and 4.15, shows the 2D field plot for the first three modes resonating inside the cavity using the solution eigenvectors. The figures shows that the field is totally confined inside the cavity.

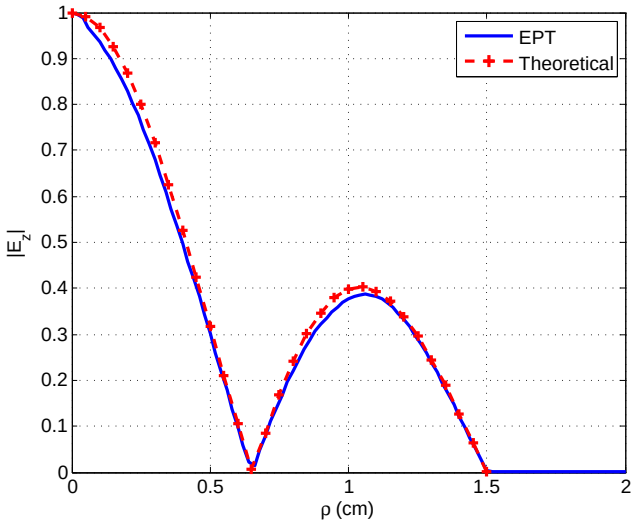

Figure 4.7: Field plot versus radial distance for TM_{02} mode of cavity of radius b=1.5 enclosed by canonical cavity of radius a=2 cm.

	Relative Error %
1^{st}Resonance	0.162441
2^{nd}Resonance	1.647522
3^{rd}Resonance	0.939483

Table 4.3: The solution relative error of the first three modes for stepped cavity with loss tangent $\tan\delta_c = 10^4$.

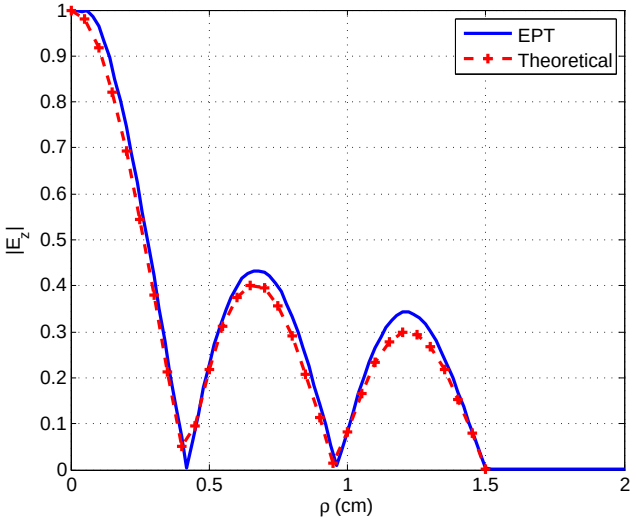

Figure 4.8: Field plot versus radial distance for TM_{03} mode of cavity of radius b=1.5 enclosed by canonical cavity of radius a=2 cm.

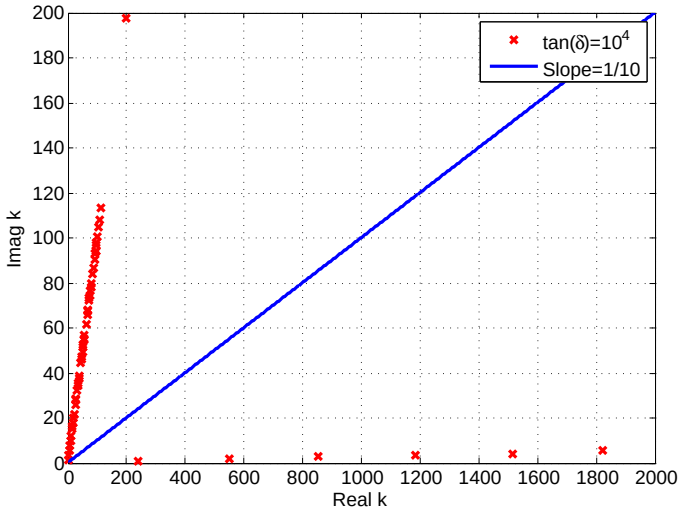

Figure 4.9: Complex propagation constant for cylindrical case with b=1, a=2 cm.

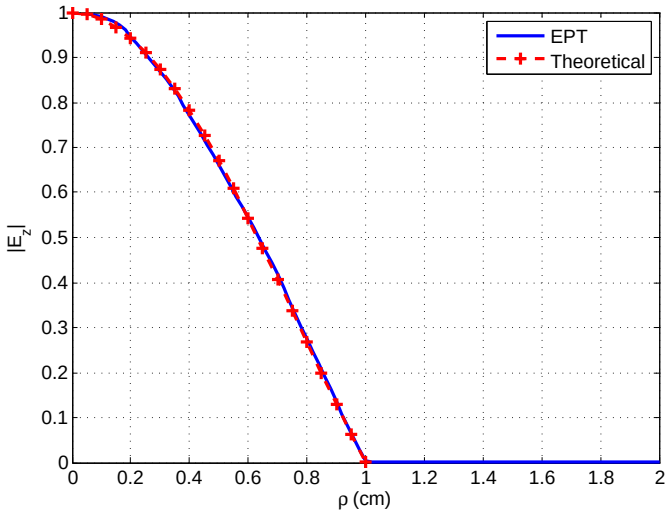

Figure 4.10: Field plot versus radial distance for TM_{01} mode of cavity of radius b=1.5 enclosed by canonical cavity of radius a=2 cm.

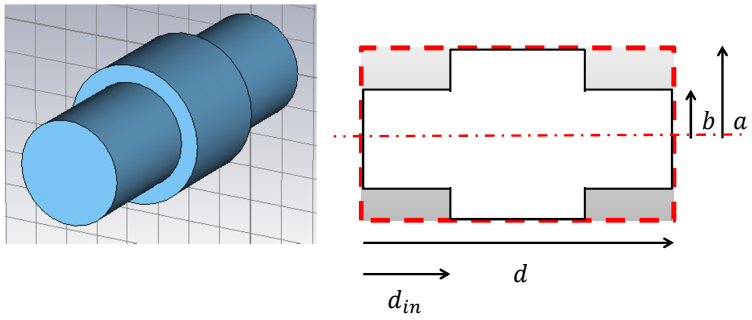

Figure 4.11: Stepped cavity enclosed by cylindrical canonical cavity.

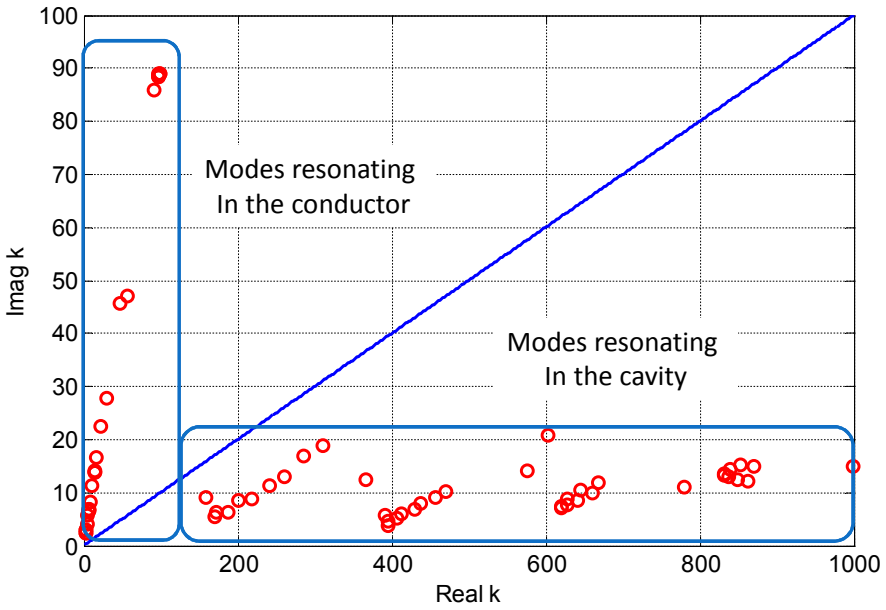

Figure 4.12: Complex propagation for stepped case with dimensions a=1.5, b=2, d_{in}=3.5 and d=10 cm.

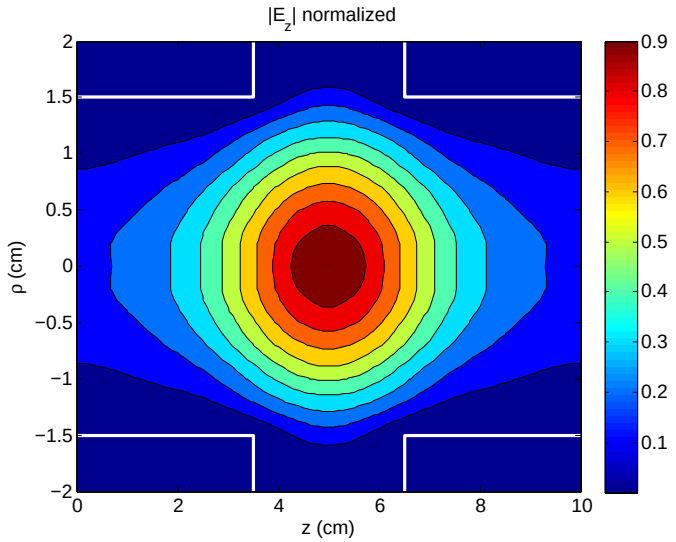

Figure 4.13: Field plot for the first TM resonance of cavity with dimensions b=2, d_{in}=3.5 and d=10 cm enclosed by canonical cavity of radius a=2 cm.

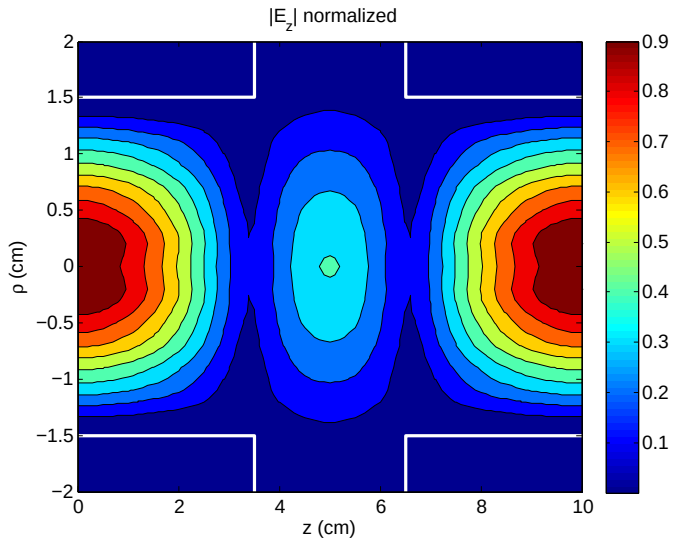

Figure 4.14: Field plot for the second TM resonance with dimensions a=1.5, b=2, d_{in}=3.5 and d=10 cm enclosed by canonical cavity of radius a=2 cm.

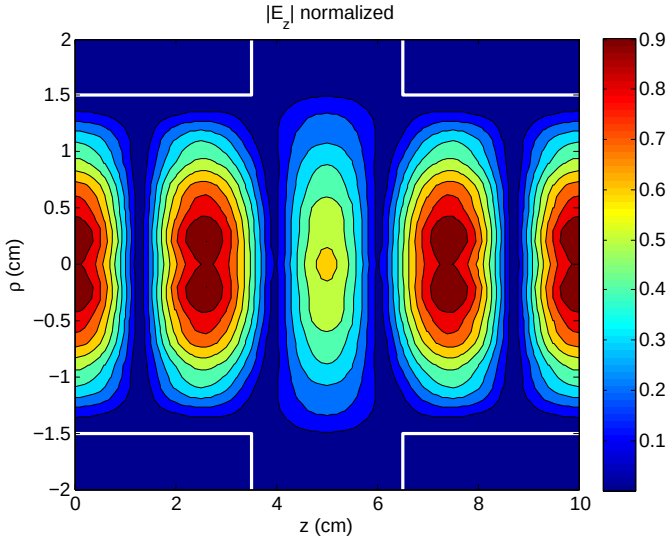

Figure 4.15: Field plot for the third TM resonance with dimensions a=1.5, b=2, d_{in}=3.5 and d=10 cm enclosed by canonical cavity of radius a=2 cm.

Chapter 5

Conclusion and Suggestions for Future Work

In this work an eigenmode projection technique was adopted in the solution of two class of problems: electromagnetic scattering from dielectric objects with complex dielectric constant and resonance of arbitrary-shaped conducting cavities.

First, the EPT was used in the analysis of electromagnetic scattering and was shown to have many advantages over the conventional numerical techniques:

- The EPT provides automatic selection of the basis functions using a complete orthogonal functions, being the eigenmodes of an enclosing fictitious canonical cavity having a geometry matching the used natural modes of free-space scattering.
- The EPT has no singularity extraction problems and does not require special treatment for the domain truncation.

Also, the unique features of the scattering solution are very useful in many ways:

- The frequency independent feature of the eigenmodes, which represent Fourier type expansion functions, results in frequency independent generated matrices is exploited to provide a solution over a wide range of frequencies efficiently without the need of filling and inverting all the system of matrices, and the encountered numerical integrations are only evaluated once, with their values used at all frequencies.
- The technique also lends itself to problems where variations of the same structure are to be analyzed, with modifications that are not necessarily small as long as they are bound by the baseline canonical cavity with the encountered numerical integrations evaluated only for the added/subtracted volume.

Second, the EPT was adopted to solve the electromagnetic resonance in an arbitrary-shaped conducting cavity and provided a solution with direct separation of the physical modes and fake (spurious) modes emerged in other previous solution approaches.

The EPT could be useful for the application of different problems in the future, and below are some suggested ideas:

- Analysis of arbitrary-shaped PEC scatterers including thin conducting sheets in free-space.
- Analysis of the problem of scattering from distant objects.
- More elaboration on the scattering from arbitrary PEC waveguide junctions.
- Analysis of radiation/antenna problems.
- Study of beam dynamics under microwave excitation with application to cavity design for high power microwave devices.

Appendix A

Detailed Formulation for the Scattering from Two Dimensional Objects

In this Appendix, the detailed formulation for the scattering from dielectric objects with complex dielectric constant will be proposed. The solution will be shown for TM^z and TE^z polarizations. The objects are excited by an incident plane wave or an impressed current source that could be inside or outside the selected fictitious canonical cavity. This cavity is chosen to be circular cavity for the addressed two dimensional problems.

It should be noted that the solenoidal cavity eigenmodes are obtained by solving (2.7) under the conditions that the differentiation $\frac{\partial}{\partial z} = 0$ due to dealing with 2D problem.

$$k_n E_{n\rho} = \frac{1}{\rho}\frac{\partial H_{nz}}{\partial \phi} \tag{A.1}$$

$$k_n E_{n\phi} = -\frac{\partial H_{nz}}{\partial \rho} \tag{A.2}$$

$$k_n E_{nz} = \frac{1}{\rho}\frac{\partial}{\partial \rho}\left(\rho H_{n\phi}\right) - \frac{1}{\rho}\frac{\partial H_{n\rho}}{\partial \phi} \tag{A.3}$$

$$k_n H_{n\rho} = \frac{1}{\rho}\frac{\partial E_{nz}}{\partial \phi} \tag{A.4}$$

$$k_n H_{n\phi} = -\frac{\partial E_{nz}}{\partial \rho} \tag{A.5}$$

$$k_n H_{nz} = \frac{\partial}{\partial \rho}\left(\rho E_{n\phi}\right) - \frac{\partial E_{n\rho}}{\partial \phi} \tag{A.6}$$

It could be noted that the system of equations could be separated into two sets as follows: first, equations (A.3-A.5) represents TM^z modes and second, equations (A.1-A.2) and (A.6) represents TE^z modes. These sets will be used to couple with incident TM^z and TE^z waves, respectively.

A.1 Scattering of TM^z Plane Wave

A.1.1 Port modes

In this problem the port modes are the summation of incident and scattered modes as follows:

$$\mathbf{E}^{port}(\mathbf{a}) = \mathbf{E}^{inc}(\mathbf{a}) + \mathbf{E}^{scat}(\mathbf{a}) \tag{A.7}$$

$$\mathbf{H}^{port}(\mathbf{a}) = -\frac{1}{j\omega\mu_0}\nabla \times \mathbf{E}^{port}(\mathbf{a}) \tag{A.8}$$

Incident Fields For TM^z plane wave propagating in a direction making angle ϕ' with x-direction, the fields could be expressed in terms of angular cylindrical harmonics. This will allow the analytical formulation. The incident electric field could be expressed as follows [21]:

$$\begin{aligned}\mathbf{E}_z^{inc} = E_{oi}e^{-jx} &= E_{oi}\sum_{p=-\infty}^{\infty} j^{-p}J_p(k\rho)e^{jp\left(\phi-\phi'\right)}\mathbf{a}_z \\ &= E_{oi}\sum_{p=0}^{\infty}\varepsilon_p j^{-p}J_p(k\rho)\cos(p\left(\phi-\phi'\right))\mathbf{a}_z, \qquad \varepsilon_p = \begin{cases} 1 & p=0 \\ 2 & otherwise \end{cases}\end{aligned} \tag{A.9}$$

where, E_{0i} is the magnitude of incident electric field and k is the propagation constant.

$\cos(p(\phi-\phi'))$ can be decomposed as follows:

$$\cos(p(\phi-\phi')) = \cos(p\phi')\cos(p\phi) + \sin(p\phi')\sin(p\phi) \tag{A.10}$$

Thus the incident modes could be represented as follows:

$$\mathbf{E}_z^{inc} = E_{oi}\sum_p \varepsilon_p j^{-p}J_p(k\rho)\mathrm{trig}(p\phi')\mathrm{trig}(p\phi)\mathbf{a}_z \tag{A.11}$$

where $\mathrm{trig}(p\phi)$ means that the summation is performed once with $\cos(p\phi)$ and another time with $\sin(p\phi)$ as follows:

$$\text{trig}(p\phi) = \begin{cases} 1 & p=0 \\ \cos(\phi) & p=1 \\ \cos(2\phi) & p=2 \\ \cos(3\phi) & p=3 \\ \vdots & \vdots \\ 0 & p=0 \\ \sin(\phi) & p=1 \\ \sin(2\phi) & p=2 \\ \sin(3\phi) & p=3 \\ \vdots & \vdots \end{cases} \tag{A.12}$$

Scattered Fields For the scattered field modes, the Hankel functions of the second kind is used to express the fields as a traveling outward fields as follows:

$$\mathbf{E}_z^{scat} = \sum_p a_p^{scat} H_p^{(2)}(k\rho)\text{trig}(p\phi)\mathbf{a}_z \tag{A.13}$$

where $\text{trig}(p\phi)$ is a summation over $\cos(p\phi)$ and $\sin(p\phi)$ with different coefficients.

Total Port Fields ($\rho = a$)

$$\mathbf{E}^{port} = \sum_{p=0}^{\infty} \left[E_{oi}\varepsilon_p j^{-p} J_P(ka)\text{trig}(p\phi') + a_p^{scat} H_p^{(2)}(ka) \right] \text{trig}(p\phi)\mathbf{a}_z \tag{A.14}$$

$$\mathbf{H}^{port} = \frac{1}{j\omega\mu_0}\left(\frac{k}{\rho} \sum_{p=0}^{\infty} p \left[E_{oi}\varepsilon_p j^{-p} J_p(ka)\text{trig}(p\phi') + a_p^{scat} H_p^{(2)}(ka) \right] \text{trig}'(p\phi)\mathbf{a}_\rho \right.$$
$$\left. + k \sum_{p=0}^{\infty} \left[E_{oi}\varepsilon_p j^{-p} J_p'(ka)\text{trig}(p\phi') + a_p^{scat} H_p^{(2)'}(ka) \right] \text{trig}(p\phi)\mathbf{a}_\phi \right) \tag{A.15}$$

$$' = \frac{\partial}{\partial(k\rho)} \tag{A.16}$$

A.1.2 Cavity Eigenmode Expansion

In this problem circular cavity with PM boundary is used. It will be shown that the choice of PM boundary eliminates (3.8) while the TM^z polarization eliminated (3.7), this will lead to a simpler solution.

Solenoidal modes As the excitation in this problem is TM^z then the excited modes inside the cavity will be TM^z modes and thus equations (A.3-A.5) are the system of equations to be solved.

Also it is obvious that $H_{n\rho}$ and $H_{n\phi}$could be obtained from E_{nz} which is obtained by solving $(\nabla^2 + k_n^2)\mathbf{E_{nz}} = 0$ (or from the above equations) and applying boundary conditions at cavity surface as follows,

$$\left(\frac{\partial^2}{\partial\rho^2} + \frac{1}{\rho}\frac{\partial}{\partial\rho} + \frac{1}{\rho^2}\frac{\partial^2}{\partial\phi^2} + k_n^2\right) E_{nz} = 0 \tag{A.17}$$

The solution of $(A.17)$ could be written as follows,

$$E_{nz} = (AJ_{n_1}(k_n\rho) + BY_{n_1}(k_n\rho))\,\mathrm{trig}(n_1\phi) \tag{A.18}$$

The function $Y_{n_1}(k_n\rho)$ is singular at $\rho = 0$ then $B = 0$ then the final expression will be as follows,

$$\mathbf{E}_n = E_{on}J_{n_1}(k_n\rho)\mathrm{trig}(n_1\phi)\mathbf{a}_z \tag{A.19}$$

where trig () is once for cos () and another for sin () with different coefficients and E_{0n} is the magnitude of cavity modes solenoidal electric fields which is obtained such that the fields are normalized with respect to the surface integral, over the fictitious cavity cross section, of the self terms i.e.$\int_{s_t} \mathbf{E}_n \cdot \mathbf{E}_n ds = \int_{s_t} \mathbf{H}_n \cdot \mathbf{H}_n ds = 1$.

Obtaining the magnetic field from the electric field equation as described previously will give the following results,

$$\mathbf{H}_n = -E_{on}\left[-\frac{n_1}{k_n\rho}J_{n_1}(k_n\rho)\frac{\partial}{\partial\phi}\mathrm{trig}(n_1\phi)\mathbf{a}_\rho + J'_{n_1}(k_n\rho)\mathrm{trig}(n_1\phi)\mathbf{a}_\phi\right] \tag{A.20}$$

Applying boundary conditions at cavity surface, then $H_\phi = 0$ at cavity surface $(\rho = a)$thus,

$$\begin{aligned} J'_{n_1}(k_n a) &= 0 \\ k_n a &= P'_{n_1 n_2} \\ k_n &= \frac{P'_{n_1 n_2}}{a} \end{aligned} \tag{A.21}$$

where, $P'_{n_1 n_2}$ is the n_2^{th} root of J'_{n_1}.

It should be noted that the indices n_1, n_2 are combined into the single index n according to the adopted numbering/sorting scheme referred to in Sec. 3.5. Similar expressions can be derived for the other field and potential quantities.

It is important here to highlight that the zero of J'_0 at the origin is not to be discarded, since J_0 is non-zero at the origin. This corresponds to a (0,0) mode studied in similar situation in [23].

It will be shown in the next section that the irrotational electric and magnetic eigenmodes coefficients vanish thus there is no need to derive them.

A.1.3 Application of Eigenmode Projections to Maxwell's Equations

In 2D problems, for equations (3.5-3.8) the volume integrals will be reduced to surface integrals and the closed surface integral will be reduced to integration on closed contour. Moreover, the problem would be much simplified using the characteristics of the current studied problem as follows:

- Dealing with PM boundary leads to vanishing $\mathbf{n} \times \mathbf{H}_n$ and Ψ_λ at surface boundary, thus the surface integral $\oint_{l_t} (\mathscr{E}^{port}(\mathbf{a};t) \times \mathbf{H}_n(\mathbf{a})) \cdot \hat{n} dl = \oint_{l_t} (\mathbf{H}_n(\mathbf{a}) \times \hat{n}) \cdot \mathscr{E}^{port}(\mathbf{a};t) dl$ in (3.5) vanishes. Also, substituting by $\Psi_\lambda = 0$ in (3.8) leads to vanishing irrotational magnetic field component for non-magnetic materials ($\mu_r(\mathbf{r}) = 1$).

- Adopting TM^z the term $\oint_{l_t} (\mathscr{E}^{port}(\mathbf{a};t)\Phi_\alpha) \cdot \mathbf{n} dl$ will no longer appear because $\mathscr{E}^{port}(\mathbf{a};t) \perp \mathbf{n}$ thus $\mathscr{E}^{port}(\mathbf{a};t) \cdot \mathbf{n} = 0$, also noting that $\mathbf{E}_{n(z)}(\mathbf{r}) \cdot \mathbf{F}_{\alpha(\rho,\phi)}(\mathbf{r}) = 0$, this will lead to vanishing of the irrotational electric field component in (3.7)

Thus the system of equations could be simplified as follows,

$$k_n a_n(t) = -\mu_0 \frac{\partial b_n(t)}{\partial t} \tag{A.22}$$

$$k_n b_n(t) + \oint_{l_t} \left(\mathscr{H}^{port}(\mathbf{r};t) \times \mathbf{E}_n(\mathbf{r})\right) \cdot \hat{n} dl = \varepsilon_0 \sum_{n'} \frac{\partial a_{n'}(t)}{\partial t} \langle \mathbf{E}_n, \mathbf{E}_{n'} \rangle \tag{A.23}$$

where,

$$\langle \mathbf{E}_n, \mathbf{E}_{n'} \rangle = \int_{s_t} \varepsilon_r(\mathbf{r}) \mathbf{E}_n(\mathbf{r}) \cdot \mathbf{E}_{n'}(\mathbf{r}) ds \tag{A.24}$$

The system of equations could be expressed in frequency domain as follows:

$$k_n a_n = -j\omega\mu_0 b_n \tag{A.25}$$

$$k_n b_n + \oint_{l_t} \left(\mathbf{H}^{port}(\mathbf{a}) \times \mathbf{E}_n(\mathbf{a})\right) \cdot \hat{n} dl = j\omega\varepsilon_0 \sum_{n'} a_{n'} \langle \mathbf{E}_n, \mathbf{E}_{n'} \rangle \tag{A.26}$$

The term $\oint_{l_t} \left(\mathbf{H}^{port}(\mathbf{a}) \times \mathbf{E}_n(\mathbf{a})\right) \cdot \mathbf{n} dl$ denoted as I_{pn} becomes

$$\begin{aligned}
I_{pn} &= \int_{\phi=0}^{2\pi} \left(\mathbf{H}^{port}(\mathbf{a}) \times \mathbf{E}_n(\mathbf{a})\right) \cdot \mathbf{a}_\rho a d\phi \\
&= \int_{\phi=0}^{2\pi} \left(\mathbf{H}_\phi^{port} \mathbf{E}_{n,z}(\mathbf{a})\right) a d\phi \\
&= \frac{ka}{j\omega\mu_0} E_{on} \int_{\phi=0}^{2\pi} \sum_p \left[E_{oi}\varepsilon_p j^{-p} J_p'(ka)\mathrm{trig}(p\phi') + a_p^{scat} H_p^{(2)'}(ka)\right] \\
&\quad \mathrm{trig}(p\phi) J_{n_1}(P'_{n_1 n_2}) \mathrm{trig}(n_1\phi) d\phi \\
&= \frac{k\gamma_{n_1} a}{j\omega\mu_0} E_{on} \left[E_{oi}\varepsilon_{n_1} j^{-n_1} J'_{n_1}(ka)\mathrm{trig}(n_1\phi') + a_{n_1}^s H_{n_1}^{(2)'}(ka)\right] J_{n_1}(P'_{n_1 n_2})
\end{aligned} \tag{A.27}$$

where,

$$\gamma_{n_1} = \begin{cases} \int_{\phi=0}^{2\pi} \cos(p\phi)\cos(n_1\phi) = 2\pi, \mathrm{trig}(n_1\phi') = 1 & n_1 = p = 0 \\ \int_{\phi=0}^{2\pi} \cos(p\phi)\cos(n_1\phi) = \pi, \mathrm{trig}(n_1\phi') = \cos(n_1\phi') & n_1 = p \neq 0 \\ \int_{\phi=0}^{2\pi} \sin(p\phi)\sin(n_1\phi) = \pi, \mathrm{trig}(n_1\phi') = \sin(n_1\phi') & n_1 = p \neq 0 \\ 0 & \text{otherwise} \end{cases} \tag{A.28}$$

Rewriting the system of equations and substituting from (A.25) and (A.27) into (A.26)

$$\begin{aligned}
-\frac{1}{j\omega\mu_0} k_n^2 a_n + \frac{k\gamma_{n_1} a}{j\omega\mu_0} E_{on} \left[E_{oi}\varepsilon_{n_1} j^{-n_1} J'_{n_1}(ka)\mathrm{trig}(p\phi') + a_{n_1}^s H_{n_1}^{(2)'}(ka)\right] J_{n_1}(P'_{n_1 n_2}) = \\
j\omega\varepsilon_0 \sum_{n'} a_{n'} \langle \mathbf{E}_n, \mathbf{E}_{n'} \rangle
\end{aligned} \tag{A.29}$$

$$\begin{aligned}
k_n^2 a_n - (k\gamma_{n_1} a) E_{on} \left[E_{oi}\varepsilon_{n_1} j^{-n_1} J'_{n_1}(ka)\mathrm{trig}(p\phi') + a_{n_1}^s H_{n_1}^{(2)'}(ka)\right] J_{n_1}(P'_{n_1 n_2}) = \\
k^2 \sum_{n'} a_{n'} \langle \mathbf{E}_n, \mathbf{E}_{n'} \rangle
\end{aligned} \tag{A.30}$$

A.1.4 Boundary Conditions Between Cavity Modes and Port Modes

Enforcing boundary conditions for electric field (non-zero at boundary) between cavity and port modes and projecting on port angular harmonics $\mathbf{h}_{p'}$ as in Sec. 3.2.4

$$\oint_S \hat{\mathbf{n}} \times \mathbf{E}^{port}(\mathbf{a}) \cdot \mathbf{h}_{p'}(\mathbf{a}) ds = \oint_S \hat{\mathbf{n}} \times \left(\sum_n a_n \mathbf{E}_n(\mathbf{a}) + \sum_\alpha f_\alpha \mathbf{F}_\alpha(\mathbf{a}) \right) \cdot \mathbf{h}_{p'}(\mathbf{a}) ds \tag{A.31}$$

Evaluating L.H.S,

$$\oint_{l_t} \mathbf{E}^{port}(a) \times \mathbf{h}_{p'}(\mathbf{a}).a_\rho a d\phi = \oint_{l_t} \sum_{p=0}^{\infty} \mathbf{e}_{pz}(a) \times \mathbf{h}_{p'\phi}(\mathbf{a}).\mathbf{a}_\rho a d\phi =$$

$$\sum_{p=0}^{\infty} - \oint_{l_t} \mathbf{e}_{p,z}(a) \mathbf{h}_{p',\phi}(\mathbf{a}) a d\phi$$

with the integral evaluated as follows:

$$\oint_{l_t} -\mathbf{e}_{p,z}(a) \mathbf{h}_{p',\phi}(\mathbf{a}) a d\phi = -\frac{ka}{j\omega\mu_0} \int_{\phi=0}^{2\pi} \left[E_{oi} \varepsilon_p j^{-p} J_p(ka) \text{trig}(p\phi') + a_p^{scat} H_p^{(2)}(ka) \right]$$

$$\left[E_{oi} \varepsilon_{p'} j^{-p'} J'_{p'}(ka) \text{trig}(p\phi') + a_{p'}^{scat} H_{p'}^{(2)'}(ka) \right] \text{trig}(p\phi) \text{trig}(p'\phi) d\phi$$

$$= -\frac{k\gamma_{p'} a}{j\omega\mu_0} \left[E_{oi} \varepsilon_p j^{-p} J_p(ka) \text{trig}(p\phi') + a_p^{scat} H_p^{(2)}(ka) \right]$$

$$\left[E_{oi} \varepsilon_{p'} j^{-p'} J'_{p'}(ka) \text{trig}(p\phi') + a_{p'}^{scat} H_{p'}^{(2)'}(ka) \right] \delta_{pp'}$$

$$\therefore \text{L.H.S} = -\frac{k\gamma_{p'} a}{j\omega\mu_0} \left[E_{oi} \varepsilon_{p'} j^{-p'} J_{p'}(ka) \text{trig}(p'\phi') + a_{p'}^{scat} H_{p'}^{(2)}(ka) \right]$$

$$\left[E_{oi} \varepsilon_{p'} j^{-p'} J'_{p'}(ka) \text{trig}(p'\phi') + a_{p'}^{scat} H_{p'}^{(2)'}(ka) \right] \tag{A.32}$$

Evaluating R.H.S,

$$\oint_{l_t}\left(\sum_n a_n\mathbf{E}_n(\mathbf{a})+\sum_\alpha f_\alpha\mathbf{F}_\alpha(\mathbf{a})\right)\times\mathbf{h}_{p'}(\mathbf{a}).\mathbf{a}_\rho a d\phi$$
$$=\sum_n a_n\oint_{l_t}\mathbf{E}_n(\mathbf{r})\times\mathbf{H}_{p'}(\mathbf{a}).\mathbf{a}_\rho a d\phi+\sum_\alpha f_\alpha\oint_{l_t}\mathbf{F}_\alpha(\mathbf{r})\times\mathbf{h}_{p'}(\mathbf{a}).\mathbf{a}_\rho a d\phi \quad (A.33)$$

with the integrals evaluated as follows:

$$\oint_{l_t}\mathbf{F}_{\alpha,(\rho,\phi)}(\mathbf{r})\times\mathbf{h}_{p',(\phi,\rho)}(\mathbf{a}).\mathbf{a}_\rho a d\phi=0 \quad (A.34)$$

Thus the irrotational modes does not couple to the radiation external field [1].

$$\oint_{l_t}\mathbf{E}_n(a)\times\mathbf{h}_{p'}(\mathbf{a}).a_\rho a d\phi=-a\oint_{l_t}\mathbf{E}_{n,z}(\mathbf{a})\mathbf{h}_{p',\phi}(\mathbf{a})d\phi$$
$$=-\frac{ka}{j\omega\mu}\int_{\phi=0}^{2\pi}\left[E_{oi}\varepsilon_{p'}j^{-p'}J'_{p'}(ka)\mathrm{trig}(p\phi')+a^s_{p'}H^{(2)'}_{p'}(ka)\right]E_{on}J_{n_1}(P'_{n_1n_2})$$
$$\mathrm{trig}(n_1\phi)\mathrm{trig}(p'\phi)d\phi \quad (A.35)$$
$$=-\frac{k\gamma_{p'}a}{j\omega\mu}\left[E_{oi}\varepsilon_{p'}j^{-p'}J'_{p'}(ka)\mathrm{trig}(p'\phi')+a^s_{p'}H^{(2)'}_{p'}(ka)\right]E_{on}J_{n_1}(P'_{n_1n_2})\delta_{p'n_1} \quad (A.36)$$

$$\therefore \text{R.H.S}=-\frac{k\gamma_{p'}a}{j\omega\mu}\left[E_{oi}\varepsilon_{p'}j^{-p'}J'_{p'}(ka)\mathrm{trig}(p'\phi')+a^s_{p'}H^{(2)'}_{p'}(ka)\right]\sum_n a_nE_{on}J_{n_1}(P'_{n_1n_2})\delta_{p'n_1} \quad (A.37)$$

Substituting from (A.32) and (A.37) into ((A.31))

$$-\frac{k\gamma_{p'}a}{j\omega\mu_0}\left[E_{oi}\varepsilon_{p'}j^{-P'}J_{P'}(ka)\mathrm{trig}(p'\phi')+a^{scat}_{p'}H^{(2)}_{P'}(ka)\right]$$
$$\left[E_{oi}\varepsilon_{p'}j^{-p'}J'_{p'}(ka)\mathrm{trig}(p'\phi')+a^{scat}_{p'}H^{(2)'}_{p'}(ka)\right]$$
$$=-\frac{k\gamma_{p'}a}{j\omega\mu_0}\left[E_{oi}\varepsilon_{p'}j^{-p'}J'_{p'}(ka)\mathrm{trig}(p'\phi')+a^{scat}_{p'}H^{(2)'}_{p'}(ka)\right]\sum_n a_nE_{on}J_{n_1}(P'_{n_1n_2})\delta_{p'n_1} \quad (A.38)$$

Thus the scattered coefficients is expressed as follows

$$a^{scat}_p=\frac{1}{H^{(2)}_P(ka)}\left[\sum_n a_nE_{on}J_{n_1}(P'_{n_1n_2})\delta_{pn_1}-E_{oi}\varepsilon_p j^{-P}J_P(ka)\mathrm{trig}(p\phi')\right] \quad (A.39)$$

In matrix form,

$$\left[a^{scat}\right]_{M\times 1} = \text{diag}\left(\frac{1}{H_P^{(2)}(ka)}\right)_{M\times M}\left[E_{on}J_{n_1}(P'_{n_1n_2})\delta_{pn_1}\right][a]_{N\times 1} - E_{0i}\left[\varepsilon_p j^{-P}\frac{J_P(ka)}{H_P^{(2)}(ka)}\text{trig}(p\phi')\right]_{M\times 1} \quad (A.40)$$

where, M and N are the number of port and solenoidal modes under consideration, respectively and diag $(v_n)$is the diagonal matrix with elements of v_n on its diagonal.

Substituting from (A.39) into (A.30) then,

$$k_n^2 a_n - (k\gamma_{n_1}a)E_{on}\left[E_{oi}\varepsilon_{n_1}j^{-n_1}J'_{n_1}(ka)\text{trig}(n_1\phi') + \frac{H_{n_1}^{(2)'}(ka)}{H_{n_1}^{(2)}(ka)}\left[\sum_m a_m E_{om}J_{m_1}(P'_{m_1m_2})\delta_{n_1m_1} - E_{oi}\varepsilon_{n_1}j^{-n_1}J_{n_1}(ka)\text{trig}(n_1\phi')\right]\right]J_{n_1}(P'_{n_1n_2}) = k^2\sum_{n'}a_{n'}\langle \mathbf{E}_n, \mathbf{E}_{n'}\rangle \quad (A.41)$$

In matrix form,

$$\left[\text{diag}\left(k_n^2\right)_{N\times N} - k^2[EE]_{N\times N} - (ka)\text{diag}\left(\gamma_{n_1}\frac{H_{n_1}^{(2)'}(ka)}{H_{n_1}^{(2)}(ka)}E_{on}J_{n_1}(P'_{n_1n_2})\right)_{N\times N}\left[E_{om}J_{m_1}(P'_{m_1m_2})\delta_{n_1m_1}\right]_{N\times N}\right][a]_{N\times 1} = \left[(k\gamma_{n_1}a)E_{on}E_{oi}\varepsilon_{n_1}j^{-n_1}\left[J'_{n_1}(ka)\text{trig}(n_1\phi') - \frac{H_{n_1}^{(2)'}(ka)}{H_{n_1}^{(2)}(ka)}J_{n_1}(ka)\text{trig}(n_1\phi')\right]J_{n_1}(P'_{n_1n_2})\right]_{N\times 1} \quad (A.42)$$

A.2 Electric Line Source Outside cavity

Electric line sources parallel to z-axis transmit electromagnetic waves with TM^z polarization, thus the solution will be much similar to the previous case but with the port field expressed as follows:

$$\mathbf{E}^{port}(\mathbf{a}) = \mathbf{E}^{imp}(\mathbf{a}) + \mathbf{E}^{scat}(\mathbf{a}) \tag{A.43}$$

$$\mathbf{H}^{port}(\mathbf{a}) = -\frac{1}{j\omega\mu_0}\nabla \times \mathbf{E}^{port}(\mathbf{a}) \tag{A.44}$$

$$\mathbf{E}_z^{imp} = E_{oi}\mathbf{a}_z \sum_{p=0}^{\infty} \varepsilon_p H_p^{(2)}(k\rho')J_p(k\rho)\text{trig}(p\phi')\text{trig}(p\phi) \tag{A.45}$$

for an impressed field due to a line source I_e located at (ρ', ϕ') with $E_0 = -I_e\frac{\omega\mu_0}{4}$ [21]. This expression is used under the condition that $\rho' > \rho$ which is valid in our case as the port fields are used to match the cavity modes at $\rho = a$ and as the line source is outside the cavity then $\rho' > a$, consequently it could be concluded that $\rho' > \rho$ [21].

The solution is then proceeded in a very similar way as scattering from TM^z plane waves with only changes in the results of the surface integrals due to the change in the excitation amplitudes.

A.3 Electric Line Source inside cavity

In this case the line source inside the canonical cavity is taken into consideration in Eq. (3.6).

A.3.1 Port Modes

In this problem the port modes are the summation of impressed and scattered modes as follows:

$$\mathbf{E}^{port}(\mathbf{a}) = \mathbf{E}^{imp}(\mathbf{a}) + \mathbf{E}^{scat}(\mathbf{a}) \tag{A.46}$$

$$\mathbf{H}^{port}(\mathbf{a}) = -\frac{1}{j\omega\mu_0}\nabla \times \mathbf{E}^{port}(\mathbf{a}) \tag{A.47}$$

The impressed electric field could be expressed as follows:

$$\mathbf{E}_z^{imp} = E_{oi}\mathbf{a}_z \sum_{p=0}^{\infty} \varepsilon_p J_p(k\rho')H_p^{(2)}(k\rho)\text{trig}(p\phi')\text{trig}(p\phi) \tag{A.48}$$

for an impressed field due to a line source I_e located at $(\rho' < \rho, \phi')$ with $E_0 = -I_e\frac{\omega\mu_0}{4}$.

Scattered field are expressed in a similar manner as scattering from TM^zplane waves, thus the total port field at $\rho = a$ could be expressed as follows:

$$\mathbf{E}_z^{port} = \sum_{p=0}^{\infty} \left[E_{oi}\varepsilon_p J_p(k\rho')\mathrm{trig}\left(p\phi'\right) + a_p^{scat} \right] \mathrm{trig}(p\phi) H_P^{(2)}(k\rho) \tag{A.49}$$

$$\mathbf{H}_\phi^{port} = \frac{k}{j\omega\mu_0} \sum_{p=0}^{\infty} \left[E_{oi}\varepsilon_p J_p(k\rho')\mathrm{trig}\left(p\phi'\right) + a_p^{scat} \right] \mathrm{trig}(p\phi) H_P^{(2)'}(k\rho) \tag{A.50}$$

A.3.2 Cavity Modes

Similar to the case of scattering of TM^z plane wave.

A.3.3 Application of Eigenmode Projections to Maxwell's Equations

The main difference than the used equations in scattering of TM^z plane wave is the existence of the current component in Eq. (3.6), thus the used equations could be expressed as follows:

$$k_n a_n(t) = -\mu_0 \frac{\partial b_n(t)}{\partial t} \tag{A.51}$$

$$k_n b_n(t) + \oint_{l_t} \left(\mathscr{H}^{port}(\mathbf{a};t) \times \mathbf{E}_n(\mathbf{a}) \right) \cdot \hat{n} dl = \varepsilon_0 \sum_{n'} \frac{\partial a_{n'}(t)}{\partial t} \langle \mathbf{E}_n, \mathbf{E}_{n'} \rangle + \int_{s_t} \mathscr{J}(\mathbf{r};t) \cdot \mathbf{E}_n(\mathbf{r}) ds \tag{A.52}$$

where,

$$\langle \mathbf{E}_n, \mathbf{E}_{n'} \rangle = \int_{s_t} \varepsilon_r(r) \mathbf{E}_n(\mathbf{r}) \cdot \mathbf{E}_{n'}(\mathbf{r}) ds \tag{A.53}$$

The system of equations could be expressed in frequency domain as follows:

$$k_n a_n = -j\omega\mu_0 b_n \tag{A.54}$$

$$k_n b_n + \oint_{l_t} \left(\mathbf{H}^{port}(\mathbf{a}) \times \mathbf{E}_n(\mathbf{a}) \right) \cdot \hat{n} dl = j\omega\varepsilon_0 \sum_{n'} a_{n'} \langle \mathbf{E}_n, \mathbf{E}_{n'} \rangle + \int_{s_t} \mathbf{J}(\mathbf{r}) \cdot \mathbf{E}_n(\mathbf{r}) ds \tag{A.55}$$

where $\mathbf{J}(\mathbf{r}) = I_e \delta_{\rho'\phi'}$, therefore the integral $\int_{s_t} \mathbf{J}(\mathbf{r}) \cdot \mathbf{E}_n(\mathbf{r}) ds = I_e \mathbf{E}_n(\rho', \phi')$.

The term $\oint_{l_t} (\mathbf{H}^{port}(\mathbf{a}) \times \mathbf{E}_n(\mathbf{a})) \cdot \mathbf{n} dl$ denoted as I_{pn} becomes

$$\begin{aligned} I_{pn} &= \int_{\phi=0}^{2\pi} \left(\mathbf{H}^{port}(\mathbf{a}) \times \mathbf{E}_n(\mathbf{a})\right) \cdot \mathbf{a}_\rho a d\phi \\ &= \int_{\phi=0}^{2\pi} \left(\mathbf{H}_\phi^{port} \mathbf{E}_{n,z}(\mathbf{a})\right) a d\phi \\ &= \frac{ka}{j\omega\mu_0} E_{on} \int_{\phi=0}^{2\pi} \sum_p \left[\varepsilon_p J_p(k\rho') \mathrm{trig}\left(p\phi'\right) + a_p^{scat}\right] \mathrm{trig}(p\phi) J_{n_1}(P'_{n_1 n_2}) \mathrm{trig}(n_1\phi) d\phi \\ &= \frac{k\gamma_{n_1} a}{j\omega\mu_0} E_{on} \left[E_{oi}\varepsilon_{n_1} J_{n_1}(ka) \mathrm{trig}(n_1\phi') + a_{n_1}^{scat}\right] J_{n_1}(P'_{n_1 n_2}) \end{aligned} \tag{A.56}$$

Rewriting the system of equations and substituting from (A.54) and (A.56) into (A.55)

$$\begin{aligned} k_n^2 a_n - (k\gamma_{n_1} a) E_{on} \left[E_{0i}\varepsilon_{n_1} J_{n_1}(k\rho') \mathrm{trig}(n_1\phi') + a_{n_1}^s\right] H_{n_1}^{(2)'}(ka) J_{n_1}(P'_{n_1 n_2}) = \\ k^2 \sum_{n'} a_{n'} \langle \mathbf{E}_n, \mathbf{E}_{n'} \rangle - j\omega\mu_0 I_e \mathbf{E}_n(\rho', \phi') \end{aligned} \tag{A.57}$$

A.3.4 Boundary Conditions Between Cavity Modes and Port Modes

Following the same procedure as in Section A.1.4 the resultant equation is as follows:

$$a_p^{scat} = \frac{1}{H_P^{(2)}(ka)} \sum_n a_n E_{on} J_{n_1}(P'_{n_1 n_2}) \delta_{pn_1} - E_{0i}\varepsilon_{p'} J_{p'}(k\rho') \tag{A.58}$$

In matrix form,

$$\left[a^{scat}\right] = diag\left(\frac{1}{H_P^{(2)}(ka)}\right)_{M\times M} \left[E_{on} J_{n_1}(P'_{n_1 n_2}) \delta_{pn_1}\right]_{M\times N} [a]_{N\times 1} - \left[E_{0i}\varepsilon_{p'} J_{p'}(k\rho')\right]_{M\times 1} \tag{A.59}$$

Substituting from (A.58) into (A.57) then,

$$k_n^2 a_n - (k\gamma_{n_1} a) E_{on} \left[E_{0i}\varepsilon_{n_1} J_{n_1}(k\rho') + \frac{1}{H_{n_1}^{(2)}(ka)} \sum_m a_m E_{om} J_{m_1}(P'_{m_1 m_2})\delta_{n_1 m_1} - E_{0i}\varepsilon_{n_1} J_{n_1}(k\rho') \right]$$
$$H_{n_1}^{(2)'}(ka) J_{n_1}(P'_{n_1 n_2}) = k^2 [EE_{nm}] a_n - j\omega\mu_0 I_e \mathbf{E}_n(\rho', \phi') \quad \text{(A.60)}$$

In matrix form,

$$\Bigg[\text{diag}\left(k_n^2\right)_{N\times N} - k^2 [EE]_{N\times N} -$$
$$(ka) * diag\left(\gamma_{n_1} \frac{H_{n_1}^{(2)'}(ka)}{H_{n_1}^{(2)}(ka)} E_{on} J_{n_1}(P'_{n_1 n_2}) \right)_{N\times N} \left[E_{om} J_{m_1}(P'_{m_1 m_2})\delta_{n_1 m_1} \right]_{N\times N} \Bigg] a_{nN\times 1}$$
$$= \left[-j\omega\mu_0 I_e \mathbf{E}_n(\rho', \phi') \right]_{N\times 1}, \quad E_{0i} = -\frac{k^2 I_e}{4\omega\varepsilon_0} \quad \text{(A.61)}$$

A.4 Scattering of TE^z Plane Wave

Taking PE boundary for the cavity surface eliminates the surface integral in (3.7), while $\mathbf{H}_{nz}$ eliminates (3.8) and thus PE boundary simplifies the solution.

The port and cavity field expressions will be the dual of the case of Scattering of TM^z plane wave and thus could be expressed as follows:

A.4.1 Port Modes

$$\mathbf{H}^{port} = \sum_{p=0}^{\infty} \left[H_{oi}\varepsilon_p j^{-p} J_P(ka)\text{trig}(p\phi') + a_p^{scat} H_p^{(2)}(ka) \right] \text{trig}(p\phi)\mathbf{a}_z \quad \text{(A.62)}$$

$$\mathbf{E}^{port} = \frac{-1}{j\omega\varepsilon_0} \Bigg(\frac{k}{\rho} \sum_{p=0}^{\infty} p \left[H_{oi}\varepsilon_p j^{-p} J_p(ka)\text{trig}(p\phi') + a_p^{scat} H_p^{(2)}(ka) \right] \frac{\partial}{\partial\phi} \text{trig}(p\phi)\mathbf{a}_\rho$$
$$+ k \sum_{p=0}^{\infty} \left[H_{oi}\varepsilon_p j^{-p} J'_p(ka)\text{trig}(p\phi') + a_p^{scat} H_p^{(2)'}(ka) \right] \text{trig}(p\phi)\mathbf{a}_\phi \Bigg) \quad \text{(A.63)}$$

$$' = \frac{\partial}{\partial(k\rho)} \quad \text{(A.64)}$$

A.4.2 Cavity Modes

It is chosen with TE^z polarization as the incident wave thus equations (A.1-A.2) and (A.6) will be used and the field expressions will be as follows:

Solenoidal modes

$$\mathbf{H}_n = H_{on} J_{n_1}(k_n \rho)\text{trig}(n_1\phi)\mathbf{a}_z \tag{A.65}$$

$$\mathbf{E}_n = -H_{on}\left[-\frac{n_1}{k_n\rho}J_{n_1}(k_n\rho)\frac{\partial}{\partial\phi}\text{trig}(n_1\phi)\mathbf{a}_\rho + J'_{n_1}(k_n\rho)\text{trig}(n_1\phi)\mathbf{a}_\phi\right] \tag{A.66}$$

where, $k_n = \frac{P'_{n_1 n_2}}{a}$ with $P'_{n_1 n_2}$ is the n_2^{th} root of J'_{n_1}.

Irrotational modes solving the wave equation $(\nabla^2 + l_\alpha^2)\phi_\alpha = 0$ and applying boundary condition at cavity surface $\phi_\alpha = 0$ (because PE boundary is utilized). The result could be expressed as follows,

$$\phi_\alpha = U_\alpha J_{\alpha_1}(k_\alpha\rho)\text{trig}(\alpha_1\phi) \tag{A.67}$$

The irrotational electric field modes is the curl of the electric potential,

$$\begin{aligned}\mathbf{F}_\alpha = \frac{1}{l_\alpha}\nabla\phi_\alpha &= \frac{1}{l_\alpha}\left[\frac{\partial}{\partial\rho}\mathbf{a}_\rho + \frac{1}{\rho}\frac{\partial}{\partial\phi}\mathbf{a}_\phi\right]\phi_\alpha \\ &= \frac{1}{l_\alpha}U_\alpha\left[k_\alpha J'_{\alpha_1}(k_\alpha\rho)\text{trig}(\alpha_1\phi)\mathbf{a}_\rho - \frac{\alpha_1^2}{\rho}J_{\alpha_1}(k_\alpha\rho)\text{trig}'(\alpha_1\phi)\mathbf{a}_\phi\right]\end{aligned} \tag{A.68}$$

where, $P_{\alpha_1\alpha_2}$ is the α_2^{th} root of J_{α_1}, $k_\alpha = \frac{P_{\alpha_1\alpha_2}}{a}$ and U_α is the magnitude of cavity modes electric scalar potential which is obtained such that the fields are normalized with respect to the surface integral of the self terms i.e. $\int_{s_t}\mathbf{F}_\alpha.\mathbf{F}_\alpha ds = \int_{s_t} U_\alpha U_\alpha ds = 1$.

It will be shown from Maxwell's equations that the coefficients $g_\lambda(t)$ will vanish thus there is no need to derive the irrotational magnetic field.

A.4.3 Application of Eigenmode Projections to Maxwell's Equations

Equations (3.5-3.8) would be much simplified using the characteristics of the current studied problem as follows:

- Dealing with PE boundary leads to vanishing $\mathbf{n}\times\mathbf{E}_n$ and ϕ_α at surface boundary, thus the surface integral $\oint_{l_t}\left(\mathscr{H}^{port}(\mathbf{r};t)\times\mathbf{E}_n(\mathbf{r})\right)\cdot\hat{n}dl=\oint_{l_t}\left(\mathbf{E}_n(\mathbf{a})\times\hat{n}\right)\cdot\mathscr{H}^{port}(\mathbf{r};t)dl$ in (3.6) vanishes. Also, Substituting by $\phi_\alpha=0$ leads to the vanishing of the term $\oint_{l_t}\left(\mathscr{E}^{port}(\mathbf{a};t)\Phi_\alpha\right)\cdot\mathbf{n}dl$ in Eq. (3.7).
- Adopting TE^z the term $\oint_{l_t}\left(\mathscr{H}^{port}(\mathbf{r};t)\psi_\lambda(\mathbf{a})\right)\cdot\mathbf{n}dl$ will no longer appear because $\mathscr{H}^{port}(\mathbf{r};t)\perp\mathbf{n}$ thus $\mathscr{H}^{port}(\mathbf{r};t)\cdot\mathbf{n}=0$ this will lead to vanishing irrotational magnetic field component by substitution in Eq. (3.8)

Thus the system of equations could be simplified as follows:

$$k_n a_n(t)+\oint_{S_t}\left(\mathscr{E}^{port}(\mathbf{a};t)\times\mathbf{H}_n(\mathbf{a})\right)\cdot ds=-\mu_0\frac{\partial b_n(t)}{\partial t} \tag{A.69}$$

$$k_n b_n(t)=\frac{\partial}{\partial t}\left[\sum_{n'}a_{n'}(t)\left\langle\mathbf{E}_n,\mathbf{E}_{n'}\right\rangle+\sum_{\alpha'}f_{\alpha'}(t)\left\langle\mathbf{E}_n,\mathbf{F}_{\alpha'}\right\rangle\right] \tag{A.70}$$

$$l_\alpha\left[\sum_{n'}a_{n'}(t)\left\langle\mathbf{E}_{n'},\mathbf{F}_\alpha\right\rangle+\sum_{\alpha'}f_{\alpha'}(t)\left\langle\mathbf{F}_\alpha,\mathbf{F}_{\alpha'}\right\rangle\right]=0 \tag{A.71}$$

Could be expressed in frequency domain as follows:

$$k_n a_n+\oint_{S_t}\left(\mathbf{E}^{port}(\mathbf{a})\times\mathbf{H}_n(\mathbf{a})\right)\cdot ds=-j\omega\mu_0 b_n \tag{A.72}$$

$$k_n b_n=j\omega\varepsilon_0\left[\sum_{n'}a_{n'}\left\langle\mathbf{E}_n,\mathbf{E}_{n'}\right\rangle+\sum_{\alpha'}f_{\alpha'}\left\langle\mathbf{E}_n,\mathbf{F}_{\alpha'}\right\rangle\right] \tag{A.73}$$

$$l_\alpha\left[\sum_{n'}a_{n'}\left\langle\mathbf{E}_{n'},\mathbf{F}_\alpha\right\rangle+\sum_{\alpha'}f_{\alpha'}\left\langle\mathbf{F}_\alpha,\mathbf{F}_{\alpha'}\right\rangle\right]=0 \tag{A.74}$$

The term $\oint_{l_t}\left(\mathbf{E}^{port}(\mathbf{a})\times\mathbf{H}_n(\mathbf{a})\right)\cdot\mathbf{n}dl$ denoted as I_{pn} becomes

$$
\begin{aligned}
I_{pn} &= \int_{\phi=0}^{2\pi} \left(\mathbf{E}^{port}(\mathbf{a}) \times \mathbf{H}_n(\mathbf{a})\right) \cdot \hat{\rho} a d\phi \\
&= \int_{\phi=0}^{2\pi} \left(\mathbf{E}_{\phi}^{port} \mathbf{H}_{nz}(\mathbf{a})\right) a d\phi \\
&= \frac{-ka}{j\omega\varepsilon_0} H_{on} \int_{\phi=0}^{2\pi} \sum_{p=0}^{\infty} \left[H_{oi}\varepsilon_p j^{-P} J_P^{'}(ka)\mathrm{trig}(p\phi') + a_p^s H_P^{(2)'}(ka)\right] \\
&\quad \mathrm{trig}(p\phi) J_{n_1}(P^{'}_{n_1 n_2})\mathrm{trig}(n_1\phi) d\phi \\
&= \frac{-k\gamma_{n_1} a}{j\omega\varepsilon_0} H_{on} \left[H_{oi}\varepsilon_{n_1} j^{-n_1} J_{n_1}^{'}(ka)\mathrm{trig}(p\phi') + a_{n_1}^s H_{n_1}^{(2)'}(ka)\right] J_{n_1}(P^{'}_{n_1 n_2})
\end{aligned} \tag{A.75}
$$

Merging the equations (A.72-A.74) and substituting with I_{pn}, leads to the following equation in matrix form:

$$
\begin{aligned}
&\left[\mathrm{diag}(k_n^2) - k^2 [Z]\right][b] = \\
&\quad [Z] \times \left[(k\gamma_{n_1} a) H_{on} \left[H_{oi}\varepsilon_{n_1} j^{-n_1} J_{n_1}^{'}(ka)\mathrm{trig}(p\phi') + a_{n_1}^{scat} H_{n_1}^{(2)'}(ka)\right] J_{n_1}(P^{'}_{n_1 n_2})\right], \\
&\qquad\qquad , [Z] = [EE] - [EF][FF]^{-1}[EF]^T
\end{aligned} \tag{A.76}
$$

A.4.4 Boundary Conditions Between Cavity Modes and Port Modes

Enforcing boundary conditions for magnetic field (non-zero at boundary) between cavity and port modes and projecting on port angular harmonics $\mathbf{e}_{p'}$ as in Sec.3.2.4:

$$
\oint_S \hat{\mathbf{n}} \times \mathbf{H}^{port}(\mathbf{a}) \cdot \mathbf{e}_{p'}(\mathbf{a}) ds = \oint_S \hat{\mathbf{n}} \times \left(\sum_n b_n \mathbf{H}_n(\mathbf{a})\right) \cdot \mathbf{e}_{p'}(\mathbf{a}) ds \tag{A.77}
$$

Following similar procedure as in Section A.1.4, the resultant equation is as follows in matrix form:

$$
\begin{aligned}
\left[a^{scat}\right]_{M\times 1} = \mathrm{diag}\left(\frac{1}{H_P^{(2)}(ka)}\right)_{M\times M} &\left[H_{on} J_{n_1}(P^{'}_{n_1 n_2})\delta_{pn_1}\right]_{M\times N} [b]_{N\times 1} \\
&- H_{0i}\left[\varepsilon_p j^{-P} \frac{J_P(ka)}{H_P^{(2)}(ka)}\right]_{M\times 1}
\end{aligned} \tag{A.78}
$$

Substituting from (A.78) into (A.76) then the final equation will be as follows,

$$\Bigg[\operatorname{diag}\left(k_n^2\right)_{N\times N} - k^2\,[Z]_{N\times N} -$$

$$(ka) * \operatorname{diag}\left(\gamma_{n_1}\frac{H_{n_1}^{(2)'}(ka)}{H_{n_1}^{(2)}(ka)}H_{on}J_{n_1}(P'_{n_1n_2})\right)_{N\times N}[Z]_{N\times N}\left[E_{om}J_{m_1}(P'_{m_1m_2})\delta_{n_1m_1}\right]_{N\times N}\Bigg][b]_{N\times 1} =$$

$$[Z]_{N\times N}\left[(k\gamma_{n_1}a)H_{on}H_{oi}\varepsilon_{n_1}j^{-n_1}\left[J'_{n_1}(ka) - \frac{H_{n_1}^{(2)'}(ka)}{H_{n_1}^{(2)}(ka)}J_{n_1}(ka)\right]J_{n_1}(P'_{n_1n_2})\right]_{N\times 1} \quad \text{(A.79)}$$

Appendix B

Outline of the Formulation for the Scattering from Three Dimensional Objects

In this Appendix, an outline of the formulation for the scattering from three dimensional objects will be proposed. The solution will be shown for TM^r and TE^r polarizations. The fictitious canonical cavity is chosen to be spherical and the solenoidal cavity eigenmodes will be represented using the vector potentials.

B.1 Solenoidal Fields in terms of Vector Potentials

Solenoidal fields are related by the following equations:

$$\nabla \times \mathbf{H}_n = k_n \mathbf{E}_n \tag{B.1}$$

$$\nabla \times \mathbf{E}_n = k_n \mathbf{H}_n \tag{B.2}$$

let

$$\mathbf{H}_n = \nabla \times \mathbf{A} \tag{B.3}$$

Substituting by (B.3) into (B.1),

$$\nabla \times \nabla \times \mathbf{A} = k_n \mathbf{E}_n \tag{B.4}$$

Substituting by (B.3) into (B.2),

$$\nabla \times \mathbf{E}_n = k_n \nabla \times \mathbf{A} \tag{B.5}$$

$$\nabla \times (\mathbf{E}_n - k_n \mathbf{A}) = 0 \tag{B.6}$$

Using the vector identity $\nabla \times (\nabla \psi) = 0$, where ψ is an arbitrary scalar potential the following equation is obtained:

$$\mathbf{E}_n - k_n \mathbf{A} = \nabla \psi \tag{B.7}$$

$$\mathbf{E}_n = k_n \mathbf{A} + \nabla \psi \tag{B.8}$$

Substituting by Eq. (B.8) into Eq. (B.4) the following equation is obtained

$$\nabla \times \nabla \times \mathbf{A} - k_n^2 \mathbf{A} = k_n \nabla \psi \tag{B.9}$$

For the TM$^{\mathrm{r}}$ polarization the solenoidal modes are constructed by letting the magnetic and electric vector potentials be equal to $\mathbf{A}(\mathbf{r}) = \hat{\mathbf{a}}_r A_r(\mathbf{r})$ and $\mathbf{F}(\mathbf{r}) = 0$, respectively.

$$\begin{aligned}\nabla \times \nabla \times \mathbf{A} =& a_r \left[-\frac{1}{r^2 \sin(\theta)} \frac{\partial}{\partial \theta} \sin(\theta) \frac{\partial A_r}{\partial \theta} - \frac{1}{r^2 \sin^2(\theta)} \frac{\partial^2 A_r}{\partial^2 \phi} \right] + \\ & a_\theta \left[\frac{1}{r} \frac{\partial^2 A_r}{\partial r \partial \theta} \right] + a_\phi \left[\frac{1}{r \sin(\theta)} \frac{\partial^2 A_r}{\partial r \partial \phi} \right]\end{aligned} \tag{B.10}$$

$$\nabla \psi = a_r \frac{\partial \psi}{\partial r} + a_\theta \frac{1}{r} \frac{\partial \psi}{\partial \theta} + a_\phi \frac{1}{r \sin(\theta)} \frac{\partial \psi}{\partial \phi} \tag{B.11}$$

Substituting by equations (B.10-B.11) into (B.9) results in the following equations:

$$-\frac{1}{r^2 \sin(\theta)} \frac{\partial}{\partial \theta} \sin(\theta) \frac{\partial A_r}{\partial \theta} - \frac{1}{r^2 \sin^2(\theta)} \frac{\partial^2 A_r}{\partial^2 \phi} - k_n^2 A_r = k_n \frac{\partial \psi}{\partial r} \tag{B.12}$$

$$\frac{1}{r} \frac{\partial^2 A_r}{\partial r \partial \theta} = k_n \frac{1}{r} \frac{\partial \psi}{\partial \theta} \tag{B.13}$$

$$\frac{1}{r \sin(\theta)} \frac{\partial^2 A_r}{\partial r \partial \phi} = k_n \frac{1}{r \sin(\theta)} \frac{\partial \psi}{\partial \phi} \tag{B.14}$$

The last two equations (B.13-B.14) are satisfied simultaneously if

$$\psi = \frac{1}{k_n} \frac{\partial A_r}{\partial r} \tag{B.15}$$

Substituting by Eq. (B.15) into Eq. (B.12)

$$\frac{1}{r^2\sin(\theta)}\frac{\partial}{\partial\theta}\sin(\theta)\frac{\partial A_r}{\partial\theta}-\frac{1}{r^2\sin^2(\theta)}\frac{\partial^2 A_r}{\partial^2\phi}-k_n^2A_r=\frac{\partial^2 A_r}{\partial r^2} \tag{B.16}$$

$$\frac{\partial^2 A_r}{\partial r^2}+\frac{1}{r^2\sin(\theta)}\frac{\partial}{\partial\theta}\sin(\theta)\frac{\partial A_r}{\partial\theta}+\frac{1}{r^2\sin^2(\theta)}\frac{\partial^2 A_r}{\partial^2\phi}+k_n^2A_r=0 \tag{B.17}$$

and can also be written in the form

$$\left(\nabla^2+k_n^2\right)\frac{A_r}{r}=0 \tag{B.18}$$

Similarly, For the TE$^{\mathrm{r}}$ polarization the solenoidal modes are constructed by letting the magnetic and electric vector potentials be equal to $\mathbf{A}(\mathbf{r})=0$ and $\mathbf{F}(\mathbf{r})=\hat{\mathbf{a}}_rF_r(\mathbf{r})$, respectively with $F_r(\mathbf{r})$ satisfying Helmholtz equation of the form:

$$\left(\nabla^2+k_n^2\right)\frac{F_r}{r}=0 \tag{B.19}$$

and $\mathbf{E}_n=\nabla\times\mathbf{F}$

B.2 Three Dimensional Solution Framework

In this case, the natural choice of the cavity will be a PE or PM spherical cavity and the eigenmodes are classified as either TM^r or TE^r. For the TM polarization, the solenoidal modes are constructed by letting the magnetic and electric vector potentials be equal to $\mathbf{A}(\mathbf{r})=\hat{\mathbf{r}}A_r(\mathbf{r})$ and $\mathbf{F}(\mathbf{r})=\mathbf{0}$, respectively [21]. The magnetic potential satisfies the Helmholtz equation of the form [24]:

$$\left(\nabla^2+k_n^2\right)\frac{A_r(\mathbf{r})}{r}=0 \tag{B.20}$$

for which the solution is given by

$$A_{r,uv}(r,\theta,\phi)=\hat{J}_u\left(k_vr\right)P_v^u\left(\cos(\theta)\right)e^{ju\phi}, \tag{B.21}$$

where $\hat{J}_n(x)$ is the Riccati Bessel function and equals $xj_n(x)$, j_n is the spherical Bessel function of order n and P_n^m is the associated Legendre functions. The solenoidal magnetic field can be readily obtained using $\mathbf{H}_n=\nabla\times(\hat{\mathbf{r}}A_r(\mathbf{r}))$ that is proved in the next section and the other field components could be obtained by substitution in (2.7). Similar expressions can be derived for scalar potentials irrotational fields. The eigenvalues k_n, l_α, w_λ are obtained by applying the boundary conditions in (3.10-3.11). Similar treatment is used for the TE^r polarization starting from the r-component of the electric vector potential. For the scattered

field modes, the spherical Hankel functions of the second kind is used to express the outgoing potentials as:

$$A_{r,p}^{scat}(r,\theta,\phi) = \hat{H}_{p_1}^{(2)}(kr)\, P_{p_1}^{p_2}(\cos(\theta))\, e^{jp_2\phi} \tag{B.22}$$

$$F_{r,p}^{scat}(r,\theta,\phi) = \hat{H}_{p_1}^{(2)}(kr)\, P_{p_1}^{p_2}(\cos(\theta))\, e^{jp_2\phi} \tag{B.23}$$

where $\hat{H}_{p_1}^{(2)}(x) = x h_{p_1}^{(2)}(x)$ and $h_{p_1}^{(2)}$ is the spherical Hankel function of the second kind and represents outgoing waves. The spherical wave transformations are used to represent the incident plane wave as illustrated in detail in [21, 24], for example an x-polarized wave propagating in the negative z-direction could be represented as

$$\mathbf{E}^{inc}(\mathbf{r}) = \hat{\mathbf{x}} E_0 e^{jkz} = \hat{\mathbf{x}} E_0 e^{jkr\cos(\theta)} = \hat{\mathbf{x}} \sum_{p=0}^{\infty} j^p (2p+1)\, j_p(kr)\, P_p(\cos(\theta)) \tag{B.24}$$

Appendix C

General Matrix Elements for the Scattering Problem Solution

Details of the matrices $[A]$ and $[B]$, and the vector $[C]$ are given in (C.3-C.5), also details of $[\Gamma(\omega)]$ and $[\Upsilon(\omega)]$ are illustrated in (C.6-C.8) and (C.9-C.11) for PM and PE cavities, respectively. It should be noted that these expressions are in the general case and could be much simplified making use of the canonical cavity boundary conditions (3.10-3.11) and the special treatment of the problem under consideration. Also, the quantity $\mathbf{E}^{exc}$ and $\mathbf{H}^{exc}$ is defined as

$$\mathbf{E}^{exc}(\mathbf{a}) = \mathbf{E}^{inc}(\mathbf{a}) + \mathbf{E}^{imp}(\mathbf{a}) \tag{C.1}$$

$$\mathbf{H}^{exc}(\mathbf{a}) = \frac{-1}{j\omega\mu_0} \nabla \times \mathbf{E}^{exc}(\mathbf{r})|_{\mathbf{a}} \tag{C.2}$$

$$[A]_{N\times N} = \left[[EE]_{N\times N} - [EF]_{N\times L}[FF]^{-1}_{L\times L}[EF]^{T}_{L\times N}\right] - \text{diag}\left(\frac{k_n^2}{\omega^2\mu_0}\right)_{N\times N} \tag{C.3}$$

$$\begin{aligned}[B]_{N\times M} = {} & \frac{\varepsilon_0}{l_\alpha}[EF]_{N\times L}[FF]^{-1}_{L\times L}\left[\oint_S (\mathbf{e}_p(\mathbf{a})\phi_\alpha(\mathbf{a}))\cdot ds\right]_{L\times M} \\ & - \frac{1}{\omega^2\mu_0}\left[\oint_S (\mathbf{e}_p(\mathbf{a})\times k_n\mathbf{H}_n(\mathbf{a}))\cdot ds\right]_{N\times M} - \frac{1}{j\omega}\left[\oint_S (\mathbf{h}_p(\mathbf{a})\times \mathbf{E}_n(\mathbf{a}))\cdot ds\right]_{N\times M}\end{aligned} \tag{C.4}$$

$$[C]_{N\times 1} = \frac{1}{\omega^2\mu_0}\left[\int_V \mathbf{M}(\mathbf{r})\cdot k_n\mathbf{H}_n(\mathbf{r})dv\right]_{N\times 1} - \frac{1}{j\omega}\left[\int_V \mathbf{J}(\mathbf{r})\cdot\mathbf{E}_n(\mathbf{r})dv\right]_{N\times 1}$$
$$+\frac{1}{\omega^2\mu_0}\left[\oint_S(\mathbf{E}^{exc}(\mathbf{a})\times k_n\mathbf{H}_n(\mathbf{a}))\cdot ds\right]_{N\times 1} + \frac{1}{j\omega}\left[\oint_S(\mathbf{H}^{exc}(\mathbf{a})\times\mathbf{E}_n(\mathbf{a}))\cdot ds\right]_{N\times 1}$$
$$-[EF]_{N\times L}[FF]^{-1}_{L\times L}\left[\varepsilon_0\oint_S\left(\mathbf{E}^{exc}(\mathbf{a})\frac{1}{l_\alpha}\phi_\alpha(\mathbf{a})\right)\cdot ds - \int_V\rho_e(\mathbf{r})\frac{1}{l_\alpha}\phi_\alpha(\mathbf{r})dv\right]_{L\times 1} \quad \text{(C.5)}$$

$$[\Gamma(\omega)]_{N\times N} = [B]_{N\times M}[Z_1]^{-1}_{M\times M}\left[\left[\oint_S\hat{\mathbf{n}}\times\mathbf{E}_n(\mathbf{a})\cdot\mathbf{h}_{p'}(\mathbf{a})ds\right]_{M\times N}\right.$$
$$\left.-\left[\oint_S\hat{\mathbf{n}}\times\mathbf{F}_\alpha(\mathbf{a})\cdot\mathbf{h}_{p'}(\mathbf{a})ds\right]_{M\times L}[FF]^{-1}_{L\times L}[EF]^T_{L\times N}\right] - \text{diag}\left(\frac{k_n^2}{\omega^2\mu_0}\right)_{N\times N} \quad \text{(C.6)}$$

$$[\Upsilon(\omega)]_{N\times 1} = [C]_{N\times 1} - [B]_{N\times M}[Z_1]^{-1}_{M\times M}\left[\left[\oint_S\hat{\mathbf{n}}\times\mathbf{F}_\alpha(\mathbf{a})\cdot\mathbf{h}_{p'}(\mathbf{a})ds\right]_{M\times L}[FF]^{-1}_{L\times L}\times\right.$$
$$\left[\varepsilon_0\oint_S\left(\mathbf{E}^{exc}(\mathbf{a})\frac{1}{l_\alpha}\phi_\alpha(\mathbf{a})\right)\cdot ds - \int_V\rho_e(\mathbf{r})\frac{1}{l_\alpha}\phi_\alpha(\mathbf{r})dv\right]_{L\times 1} -$$
$$\left.\left[\oint_S\hat{\mathbf{n}}\times\mathbf{E}^{exc}(\mathbf{a})\cdot\mathbf{h}_{p'}(\mathbf{a})ds\right]_{M\times 1}\right] \quad \text{(C.7)}$$

$$[Z_1]_{M\times M} = \left[\oint_S\hat{\mathbf{n}}\times\mathbf{e}_p(\mathbf{a})\cdot\mathbf{h}_{p'}(\mathbf{a})ds\right]_{M\times M} -$$
$$\varepsilon_0\left[\oint_S\hat{\mathbf{n}}\times\mathbf{F}_\alpha(\mathbf{a})\cdot\mathbf{h}_{p'}(\mathbf{a})ds\right]_{M\times L}[FF]^{-1}_{L\times L}\left[\oint_S\left(\mathbf{e}_p(\mathbf{a})\frac{1}{l_\alpha}\phi_\alpha(\mathbf{a})\right)\cdot ds\right]_{L\times M} \quad \text{(C.8)}$$

$$[\Gamma(\omega)]_{N\times N} = \frac{-1}{j\omega\mu_0}[B]_{N\times M}[Z_2]^{-1}_{M\times M}\left[\oint_S\hat{\mathbf{n}}\times k_n\mathbf{H}_n(\mathbf{a})\cdot\mathbf{e}_{p'}(\mathbf{a})ds\right] - \text{diag}\left(\frac{k_n^2}{\omega^2\mu_0}\right)_{N\times N} \quad \text{(C.9)}$$

$$
\begin{aligned}
[\Upsilon(\omega)]_{N\times 1} = [C]_{N\times 1} - [B]_{N\times M}\,[Z_2]^{-1}_{M\times M} \times \\
\left[\frac{-1}{j\omega\mu_0}\left[\oint_S \hat{\mathbf{n}}\times\mathbf{H}_n(\mathbf{a})\cdot\mathbf{e}_{p'}(\mathbf{a})ds\right]_{M\times N}\left[\oint_S (\mathbf{E}^{exc}(\mathbf{a})\times\mathbf{H}_n(\mathbf{a}))\cdot ds + \int_V \mathbf{M}(\mathbf{r})\cdot\mathbf{H}_n(\mathbf{r})dv\right]_{N\times 1}\right. \\
+\left[\oint_S \hat{\mathbf{n}}\times\mathbf{G}_\alpha(\mathbf{a})\cdot\mathbf{e}_{p'}(\mathbf{a})ds\right]_{M\times O}\left[\oint_S\left(\mathbf{H}^{exc}(\mathbf{a})\frac{1}{w_\lambda}\psi_\lambda(\mathbf{a})\right)\cdot ds - \frac{1}{\mu_0}\int_V \rho_m(\mathbf{a})\psi_\lambda(\mathbf{r})dv\right]_{O\times 1} \\
\left.-\left[\oint_S \hat{\mathbf{n}}\times\mathbf{H}^{exc}(\mathbf{a})\cdot\mathbf{e}_{p'}(\mathbf{a})ds\right]_{M\times 1}\right] \qquad \text{(C.10)}
\end{aligned}
$$

$$
\begin{aligned}
[Z_2]_{M\times M} = \left[\oint_S \hat{\mathbf{n}}\times\mathbf{h}_p(\mathbf{a})\cdot\mathbf{e}_{p'}(\mathbf{a})ds\right]_{M\times M} + \\
\frac{1}{j\omega\mu_0}\left[\oint_S \hat{\mathbf{n}}\times\mathbf{H}_n(\mathbf{a})\cdot\mathbf{e}_{p'}(\mathbf{a})ds\right]_{M\times N}\left[\oint_S (\mathbf{e}_p(\mathbf{a})\times\mathbf{H}_n(\mathbf{a}))\cdot ds\right]_{N\times M} - \\
\left[\oint_S \hat{\mathbf{n}}\times\mathbf{G}_\lambda(\mathbf{a})\cdot\mathbf{e}_{p'}(\mathbf{a})ds\right]_{M\times O}\left[\oint_S\left(\mathbf{h}_p(\mathbf{a})\frac{1}{w_\lambda}\psi_\lambda(\mathbf{a})\right)\cdot ds\right]_{O\times M} \qquad \text{(C.11)}
\end{aligned}
$$

and the matrices $[EE]_{N\times N}$, $[EF]_{N\times L}$ and $[FF]_{L\times L}$ hold as their elements the cavity eigenmode projections $\langle\mathbf{E}_n, \mathbf{E}_{n'}\rangle$, $\langle\mathbf{E}_n, \mathbf{F}_\alpha\rangle$ and $\langle\mathbf{F}_\alpha, \mathbf{F}_{\alpha'}\rangle$, respectively.

Appendix D

Boundary Conditions between Cavity Eigenmodes and Port Modes

For the cavity field expansion (3.3-3.4) to be used directly inside the surface integral in (3.10-3.11), the following relation will be proved for canonical cavity with PE boundary:

$$\oint_S \hat{\mathbf{n}} \times \mathbf{E}^{port}(\mathbf{a}) \cdot \mathbf{h}_{p'}(\mathbf{a}) ds = \oint_S \hat{\mathbf{n}} \times \left(\sum_n a_n \mathbf{E}_n(\mathbf{a}) + \sum_\alpha f_\alpha \mathbf{F}_\alpha(\mathbf{a}) \right) \cdot \mathbf{h}_{p'}(\mathbf{a}) ds \tag{D.1}$$

Before arriving at the equations resulting from the boundary conditions, it is important to emphasize that the expansion,

$$\mathbf{E}^{cav}(\mathbf{r}) = \sum_n a_n \mathbf{E}_n(\mathbf{r}) + \sum_\alpha f_\alpha \mathbf{F}_\alpha(\mathbf{r}) \tag{D.2}$$

is understood in the volume-integral sense, i.e. (D.2) means that for an arbitrary bounded vector function $\mathbf{F}$,

$$\int_V \mathbf{E}^{cav} \cdot \mathbf{F} dv = \int_V \left(\sum_n a_n \mathbf{E}_n + \sum_\alpha f_\alpha \mathbf{F}_\alpha \right) \cdot \mathbf{F} dv \tag{D.3}$$

A closed surface integral can be transformed into a volume integral using the divergence theorem as

$$\oint_S \hat{\mathbf{n}} \times \mathbf{E}^{cav} \cdot \mathbf{h}_{p'} ds = \int_V \left(\nabla \times \mathbf{E}^{cav} \cdot \mathbf{h}_{p'} - \mathbf{E}^{cav} \cdot \nabla \times \mathbf{h}_{p'} \right) dv \tag{D.4}$$

Now the expansion for $\mathbf{E}^{cav}$ and $\nabla \times \mathbf{E}^{cav}$ can be substituted in the volume integral. Similar to the field expansion for $\mathbf{E}^{cav}$ in (D.2), the expansion for $\nabla \times \mathbf{E}^{cav}$, after some manipulation [1, 2] can be written as,

$$\nabla \times \mathbf{E}^{cav} = \sum_n \left(k_n a_n + \oint_S \mathbf{n} \times \mathbf{E}^{cav} \cdot \mathbf{H}_n ds \right) \mathbf{H}_n + \sum_\alpha \left(\oint_S \mathbf{n} \times \mathbf{E}^{cav} \cdot \mathbf{G}_\alpha ds \right) \mathbf{G}_\alpha \tag{D.5}$$

Using the boundary conditions in (3.10) for PM cavity, (D.5) can be simplified to,

$$\nabla \times \mathbf{E}^{cav} = \sum_n k_n a_n \mathbf{H}_n = \sum_n a_n \nabla \times \mathbf{E}_n = \nabla \times \left(\sum_n a_n \mathbf{E}_n + \sum_\alpha f_\alpha \mathbf{F}_\alpha \right) \tag{D.6}$$

where the fact that the irrotational eigenmodes are curl-free was used to reach the previous expression.

Substituting with the expansions of $\nabla \times \mathbf{E}^{cav}$ and $\mathbf{E}^{cav}$, equations (D.2) and (D.6), respectively, into the volume integral in (D.4), yields

$$\begin{aligned} \oint_S \hat{\mathbf{n}} \times \mathbf{E}^{cav} \cdot \mathbf{h}_{p'} ds &= \int_V \left[\nabla \times \left(\sum_n a_n \mathbf{E}_n + \sum_\alpha f_\alpha \mathbf{F}_\alpha \right) \cdot \mathbf{h}_{p'} - \left(\sum_n a_n \mathbf{E}_n + \sum_\alpha f_\alpha \mathbf{F}_\alpha \right) \cdot \nabla \times \mathbf{h}_{p'} \right] dv \\ &= \int_V \nabla \cdot \left[\left(\sum_n a_n \mathbf{E}_n + \sum_\alpha f_\alpha \mathbf{F}_\alpha \right) \times \mathbf{h}_{p'} \right] dv \end{aligned} \tag{D.7}$$

The divergence theorem can be applied to (D.7), which gives

$$\oint_S \hat{\mathbf{n}} \times \mathbf{E}^{cav}(\mathbf{a}) \cdot \mathbf{h}_{p'}(\mathbf{a}) ds = \oint_S \hat{\mathbf{n}} \times \left(\sum_n a_n \mathbf{E}_n(\mathbf{a}) + \sum_\alpha f_\alpha \mathbf{F}_\alpha(\mathbf{a}) \right) \cdot \mathbf{h}_{p'}(\mathbf{a}) ds$$

Hence the proof is complete. It can be proved similarly that for canonical cavity with PE boundary

$$\oint_S \hat{\mathbf{n}} \times \mathbf{H}^{port}(\mathbf{a}) \cdot \mathbf{e}_{p'}(\mathbf{a}) ds = \oint_S \hat{\mathbf{n}} \times \left(\sum_n b_n \mathbf{H}_n(\mathbf{a}) + \sum_\lambda g_\lambda \mathbf{G}_\lambda(\mathbf{a}) \right) \cdot \mathbf{e}_{p'}(\mathbf{a}) ds \tag{D.8}$$

References

[1] J. C. Slater, *Microwave Electronics*. D Van Nostrand Company, 1950.

[2] K. Kurokawa, "The expansions of electromagnetic fields in cavities," *IEEE Trans. Microwave Theory Techn.*, vol. 6, pp. 178–187, April 1955.

[3] S. Schelkunoff, "Representation of impedance functions in terms of resonant frequencies," *Proceedings of the IRE*, vol. 32, pp. 83 – 90, feb. 1944.

[4] T. Teichmann and E. P. Wigner, "Electromagnetic field expansions in loss-free cavities excited through holes," *Journal of Applied Physics*, vol. 24, pp. 262 –267, mar 1953.

[5] S. A. Schelkunoff, "On representation of electromagnetic fields in cavities in terms of natural modes of oscillation," *Journal of Applied Physics*, vol. 26, pp. 1231 –1234, oct 1955.

[6] S. Cohn, "Design considerations for high-power microwave filters," *Microwave Theory and Techniques, IRE Transactions on*, vol. 7, pp. 149 –153, january 1959.

[7] A. Wexler, "Solution of waveguide discontinuities by modal analysis," *Microwave Theory and Techniques, IEEE Transactions on*, vol. 15, pp. 508 –517, september 1967.

[8] R. MacPhie and K.-L. Wu, "A full-wave modal analysis of arbitrarily shaped waveguide discontinuities using the finite plane-wave series expansion," *Microwave Theory and Techniques, IEEE Transactions on*, vol. 47, pp. 232 –237, feb 1999.

[9] D.-C. Liu, "On the theory of the modal expansion method for the em fields inside a closed volume," *Journal of Physics D: Applied Physics*, vol. 36 no. 13, p. 1629, 2003.

[10] R. MacPhie and K.-L. Wu, "A plane wave expansion of spherical wave functions for modal analysis of guided wave structures and scatterers," *Antennas and Propagation, IEEE Transactions on*, vol. 51, pp. 2801 – 2805, oct. 2003.

[11] F. Moglie, T. Rozzi, P. Marcozzi, and A. Schiavoni, "A new termination condition for the application of fdtd techniques to discontinuity problems in close homogeneous waveguide," *Microwave and Guided Wave Letters, IEEE*, vol. 2, pp. 475 –477, dec. 1992.

[12] Z. Lou and J.-M. Jin, "An accurate waveguide port boundary condition for the time-domain finite-element method," *Microwave Theory and Techniques, IEEE Transactions on*, vol. 53, pp. 3014 – 3023, sept. 2005.

[13] A. Belenguer, H. Esteban, V. Boria, C. Bachiller, and J. Morro, "Hybrid mode matching and method of moments method for the full-wave analysis of arbitrarily shaped structures fed through canonical waveguides using only electric currents," *Microwave Theory and Techniques, IEEE Transactions on*, vol. 58, pp. 537 –544, march 2010.

[14] M. Othman, T. Abuelfadl, and I. Eshrah, "Analysis of microwave cavities using an eigenmode projection approach," in *Antennas and Propagation Society International Symposium (APSURSI), 2012 IEEE*, pp. 1–2, 2012.

[15] M. Othman, I. Eshrah, and T. Abuelfadl, "Analysis of waveguide discontinuities using eigenmode expansion," in *Microwave Symposium Digest (MTT), 2013 IEEE MTT-S International*, 2013.

[16] R. Harrington, *Field Computation by Moment Methods*. IEEE/OUP Series on Electromagnetic Wave Theory, Oxford University Press, USA, 1993.

[17] K. Kunz and R. Luebbers, *The Finite Difference Time Domain Methods for Electromagnetics*. Taylor & Francis, 1993.

[18] R. E. Collin, *Foundationws for Microwave Engineering*. IEEE Press Series on Electromagnetic Wave Theory, Wiely-Interscience, 2001.

[19] M. Othman, I. Eshrah, and T. Abuelfadl, "Solution of electromagnetic scattering and resonance problems using cavity modal expansion," *MSc thesis, Dep. of Electronics and Electrical Communications, Faculty of Engineering, Cairo University*, 2012.

[20] K. S. Miller, "On the inverse of the sum of matrices," *Mathematics Magazine*, vol. 54, pp. 69–70, March 1981.

[21] C. A. Balanis, *Advanced Engineering Electromagnetics*. John Wiley & Sons Inc., 1989.

[22] C. A. Balanis, *Antenna theory: analysis and design*. JOHN WILET & SONS, INC., 1997.

[23] I. Eshrah, A. Yakovlev, A. Kishk, A. Glisson, and G. Hanson, “The te00 waveguide mode - the "complete" story,” *Antennas and Propagation Magazine, IEEE*, vol. 46, no. 5, pp. 33–41, 2004.

[24] R. Harrington, *Time-Harmonic Electromagnetic Fields*. IEEE Press Series on Electromagnetic Wave Theory, Wiley, 2001.